Dynacortin, a Genetic Link between Equatorial Contractility and Global Shape Control Discovered by Library Complementation of a *Dictyostelium discoideum* Cytokinesis Mutant

Douglas N. Robinson and James A. Spudich

Department of Biochemistry and Developmental Biology, Beckman Center, Stanford University, Stanford, California 94305-5307

Abstract. We have developed a system for performing interaction genetics in *Dictyostelium discoideum* that uses a cDNA library complementation/multicopy suppression strategy. Chemically mutagenized cells were screened for cytokinesis-deficient mutants and one mutant was subjected to library complementation. Isolates of four different genes were recovered as modifiers of this strain's cytokinesis defect. These include the cleavage furrow protein cortexillin I, a novel protein we named dynacortin, an ezrin-radixin-moesin-family protein, and coronin. The *cortexillin I* locus and transcript were found to be disrupted in the strain, identifying it as the affected gene. Dynacortin is localized partly to the cell cortex and becomes enriched in protrusive regions, a localization pattern that is similar to coronin and partly dependent on RacE. During cytokinesis, dynacortin is found in the cortex and is somewhat enriched at the poles. Furthermore, it appears to be reduced in the cleavage furrow. The genetic interactions and the cellular distributions of the proteins suggest a hypothesis for cytokinesis in which the contraction of the medial ring is a function of spatially restricted cortexillin I and myosin II and globally distributed dynacortin, coronin, and RacE.

Key words: cytoskeleton • cortexillin • cell cortex • cell protrusion • Rac small GTPase

Introduction

Cytokinesis is the process by which a cell divides into two daughter cells. Over the past century, several studies have helped to uncover the cellular mechanisms of cytokinesis. The following general theme for cytokinesis has emerged from studies on organisms ranging from yeast and amoeboid cells to echinoderm eggs and mammalian cells. The astral and/or interdigitating microtubules from the mitotic spindle send a signal to the equatorial cortex, triggering its contraction. This creates a cortical tension gradient in which the peak of the tension occurs at the equator and the lowest point of tension occurs at the cell poles. This leads to the constriction of the cell at the equator, cleaving the cell into two daughter cells (for review see Rappaport, 1996; Robinson and Spudich, 2000).

However, until recently, the molecular basis of cytokinesis has remained largely elusive, due in large part to the transient nature of the process compared with the length of the cell cycle. The conventional nonmuscle myosin II (myo II)[1] contributes substantially to the equatorial contractile force in a number of organisms (for example, DeLozanne and Spudich, 1987; McCollum et al., 1995; Bezanilla et al., 1997; Kitayama et al., 1997), but it might not be the sole contributor to equatorial contractile force generation. In the cellular slime mold, *Dictyostelium discoideum*, myo II mutant cells are capable of cleaving into two cells if cells are grown on surfaces. In mammals, myosin Is of the brush border subfamily are also localized to the cleavage furrow (Breckler and Burnside, 1994; Ruppert et al., 1995), and in *Schizosaccharomyces pombe*, two different conventional myo IIs can be found in the cleavage furrow (Bezanilla et al., 1997; Kitayama et al., 1997).

Nonmotor proteins have been shown to generate cortical tension and regulate cell shape. In *D. discoideum*, cortexillins encoded by the *cortexillin I* and *II* genes are required for cytokinesis (Faix et al., 1996). The cortexillins consist of an NH_2-terminal spectrin-family actin binding domain, a coiled-coil domain, and a COOH-terminal do-

Address correspondence to Douglas N. Robinson, Department of Biochemistry and Developmental Biology, Beckman Center, Rm. B-400, Stanford University, Stanford, CA 94305-5307. Tel.: 650-725-6376. Fax: 650-725-6044. E-mail: drobinso@cmgm.stanford.edu

[1]*Abbreviations used in this paper:* myo II, myosin II; *myo II*$^-$, myo II null cell line; NQNO, 4-nitroquinolone-*N*-oxide; NaV_i, sodium vanadate (Na_2HVO_4); ORF, open reading frame.

main that has actin filament-bundling activity and a PIP_2-binding site. Cortexillin I localizes to the cleavage furrow and the COOH-terminal domain is sufficient for cortexillin I's function in cytokinesis (Weber et al., 1999). This COOH-terminal domain is also sufficient for actin filament bundling in vitro (Stock et al., 1999). Loss of cortexillin function leads to a reduction in cortical tension (Simson et al., 1998). *D. discoideum* coronin is an actin filament-crosslinking protein that is required to maintain cell shape and loss of it leads to defects in cytokinesis (deHostas et al., 1991, 1993). Mutations in the *RacE* small GTPase gene lead to reduced general cortical tension and failure in cytokinesis, implicating a signaling cascade that modulates cortical tension (Larochelle et al., 1997; Gerald et al., 1998).

In recent years, many new proteins have been identified that are involved in or required for cytokinesis. Many of these proteins have been discovered in *D. discoideum*, yeast, *Caenorhabditis elegans*, and *Drosophila melanogaster*. Only the cellular slime mold, *D. discoideum*, offers development and metazoan-type cellular physiology, as well as good cytology for microscopy, molecular genetic methods including insertional mutagenesis, and the ability to produce preparative quantities of cells for biochemical analyses (for review see Kay and Williams, 1999). However, complex genetic interactions between molecules are still difficult to probe. This is due in part to the lack of a meiotic phase in laboratory *D. discoideum* strains, which restricts the ability to map mutations by recombination and greatly inhibits the ability of using genetic recombination to identify epistatic relationships. To dissect further the molecular mechanisms of cytokinesis, we have developed library complementation and high copy suppression methods to perform interaction genetics in *D. discoideum*. This has allowed us to identify a novel gene, dynacortin, which plays a role in the function of a dynamic cell cortex and interacts genetically between regional and global cortical tension generating pathways that are necessary for efficient cleavage of the cell.

Materials and Methods

D. discoideum Strains and Cell Culture

For an isogenic parental wild-type strain for the mutagenesis experiments, a single subclone (ORF+7-3; HS1000) of ORF+ cells (Manstein et al., 1995) was isolated (Table I). The ORF+ cell line was chosen because it contains the pRep open reading frame (ORF), which is stably integrated in the genome. The pRep ORF is required for the replication of Ddp2 replication origins in *D. discoideum*, and can function in trans (Chang et al., 1990; Slade et al., 1990). Having the ORF integrated in the genome allows Ddp2-based episomal vectors to be transformed into *D. discoideum* cells without the use of the helper pRep plasmid.

The myo II null cell line (*myo II*$^-$) was generated by using gene replacement to remove the *D. discoideum myo II heavy chain A* (*mhcA*) gene from the wild-type JH10 strain (Ruppel et al., 1994). The *RacE* null cell line (p69C5-3G1) used has a complete deletion of the *RacE* gene (Table I). The *RacE*$^-$ 24EH6 strain is a restriction enzyme-mediated plasmid integration mutant and the wild-type DH1 cells used in this study are the exact parental strain used to generate 24EH6 (Larochelle et al., 1996). The Δ*cortI* strain is a deletion of the *cortexillin I* locus generated by homologous recombination in the wild-type Ax2 background (Faix et al., 1996).

D. discoideum ORF+7-3–derived strains were grown in Hans' enriched HL-5 media (1.4× HL-5, 8% FM) plus penicillin (60 U/ml), streptomycin sulfate (60 μg/ml), and plus or minus G418 (15 μg/ml), depending on whether the cells are transformed with an episomal plasmid. Ax2-214 and JH10 derivatives with episomal plasmids were grown in 10 μg/ml G418 or 4 μg/ml blasticidin, as appropriate. DH1, 24EH6, and p69C5-3G1 derivatives with episomal plasmids were grown in 7.5 μg/ml G418. Cells were propagated at 22°C on 10-cm plates. For suspension growth assays, cells were grown in 25-ml culture volumes in 250-ml Erlenmeyer flasks at 180 rpm. Cell densities were determined using a hemacytometer.

Mutagenesis and Mutant Screening of D. discoideum Cells

For mutagenesis, we modified the protocol described by Patterson and Spudich (1995). Log phase ORF+7-3 cells were harvested and resuspended in MES starvation buffer (50 mM MES, pH 6.8, 2 mM $MgCl_2$, 0.2 mM $CaCl_2$). 4-nitroquinolone-*N*-oxide (NQNO; Sigma-Aldrich) was added to 12 μg/ml. Cells were incubated in the NQNO for 30 min with gentle rocking. 35% of the cells survived at this dose of NQNO. Cells were washed twice in 5 ml of standard HL-5 media. Cells were plated at a density of 5,000 cells/well in 26 6-well tissue culture plates (Falcon; Becton Dickinson). Approximately 273,000 genomes were examined. Cells were grown for 3 to 4 d at 22°C and then shifted to 13°C for 3 to 4 d. Using a 32× magnification, wells were screened for clusters of cells with an increased number of large cells. The clusters were transferred to a fresh 6-well plate and grown up as before. The cells were passaged and screened 3 to 4 times until they appeared to be clonal. The cells were then plated on *Klebsiella aerogenes* lawns to select for single clones and to assay for developmental phenotypes.

For further examination of a cytokinesis phenotype, cell lines were grown in suspension culture in 25-ml cultures in 250-ml Erlenmeyer flasks at 180 rpm. We find that growth under these conditions increases the penetrance of any cytokinesis defect, resulting in multinucleated cells. Cell lines were analyzed for the nuclei/cell ratio distribution, growth rate, smoothness of the growth curve, and saturation density. A high nuclei/cell ratio and a lower saturation density are indicative of a cytokinesis defect.

Table I. D. discoideum Strains Used in This Paper

Strain	Genotype	Genetic modification	Reference
HS1	Δ*mhcA*	Deletion of *mhcA* locus in JH10 cells (referred to as *myo II*$^-$)	Ruppel et al., 1994
DH1	*ura*$^-$	Wild-type parental strain for 24EH6	Larochelle et al., 1996
24EH6	*RacE*$^-$	REMI insertion in *RacE* gene	Larochelle et al., 1996
p69C5-3G1	Δ*RacE*	Deletion of the *RacE* gene	DeLozanne, A., personal communication
Ax2-214	Wild-type	Wild-type parent for the ΔcortI-214 strain	Faix et al., 1996
ΔcortI-214	Δ*cortI*	Deletion of the *cortexillin I* locus	Faix et al., 1996
Ax3:ORF+	Wild-type; REP ORF+	Ddp2 origin replicase ORF integrated in genome (wild-type otherwise)	Morandini, P., and R. Kay, personal communication; Manstein et al., 1995
HS1000	Ax3; ORF+7-3	Subclone 7-3 of Ax3:ORF+ cells used as wild-type parental strain for this study	This paper
HS1151	$cortI^{11\text{-}5.1}$	NQNO induced deletion in HS1000 that removes the *cortexillin I* locus	This paper

Plasmids

The expression vector used for library expression, pLD1A15SN, was modified from a vector, pLD1, which contains the Ddp2-based origin of replication (Chang et al., 1990; Slade et al., 1990). The vector contains the actin-15 promoter with no ATG and the actin-15 transcription termination region. The following polylinker was introduced:

→ Transcription start SalI
AATTAAATAAAAAAATAAAA GTCGAC T ACTAGT T
NotI Stop codons MluI
GCGGCCGCTAAATAAATAAACGCGT.

A GFP (S65T)-tagging cassette was generated in pBlueScript-II+SK that allows one to easily construct cDNA fragments with the GFP sequence fused at the 5′ or 3′ end for NH_2-terminal or COOH-terminal GFP fusions, respectively. The GFP (S65T)-tagging cassette can be moved easily as a SalI-NotI fragment into pLD1A15SN. In this manner, the GFP fusion proteins described below were constructed.

pLD1A15SN:GFP-dynacortin and pLD1A15SN:coronin-GFP were constructed using PCR, cloning into the GFP (S65T)-tagging cassette and subcloning into pLD1A15SN. A blasticidin resistant-dynacortin 2B19 expressing plasmid was generated using PCR to generate a cDNA with appropriate restriction consensus sites and subcloning the fragment into a modified pDXA-3H vector (Manstein et al., 1995) called pDXA-3H-Bl. This vector has had the G418-resistance marker replaced with a blasticidin-resistance marker (a gift from G. Cavet and J.A. Spudich).

Library Construction

A *D. discoideum* expression library was generated using the pLD1A15SN expression vector (Fig. 1). Total RNA was purified from axenically surface-grown and suspension-grown Ax2 cells, using the TRIzol extraction method (GIBCO BRL). The RNA from the two populations was quantitated by ultraviolet optical density spectroscopy and mixed in a 50:50 ratio. PolyA+ RNA was purified by selecting two times sequentially with oligo(dT)-cellulose type 2 (Collaborative Research Inc.) using standard techniques. The RNA quality was verified by appearance on an ethidium bromide-stained formaldehyde-agarose gel and by hybridization with a single labeled 3-kb gene to the RNA immobilized on a nylon membrane.

PolyA+ mRNA was converted into cDNA ready for ligation into pLD1A15SN using the SuperScript plasmid system for cDNA synthesis and plasmid cloning kit (GIBCO BRL). This system incorporates a SalI and MluI restriction sites at the 5′ end and a NotI restriction site at the 3′ end of the cDNAs. The cDNAs were ligated into the SalI and NotI restriction sites of pLD1A15SN. Since *D. discoideum* has a high AT content, which can cause the *D. discoideum* DNA sequences to be unstable in many *Escherichia coli* strains, the ligated plasmids were transformed into MaxEfficiency STBL2 cells (GIBCO BRL) and grown at 30°C to help stabilize the plasmids. A minimum of 250,000 bacterial transformants was recovered and analysis revealed that a minimum of 80% of the plasmid clones contained inserts. The average insert size was 1.1–1.3 kb, and the size ranged from 0.5 to >4 kb.

Library plasmid DNA was generated from 700,000–800,000 colony forming units. Colonies were allowed to grow on the plates and were harvested. Plasmid DNA was recovered, divided into two parts, and purified on a Maxi-Prep ion exchange resin (Qiagen Inc.).

Transformation of the Plasmid Library into D. discoideum Cells

In a typical experiment, mutant *D. discoideum* cells were grown on 20 10-cm plates in Hans' enriched HL-5 and collected during log phase growth. Cells were pooled and washed one time in 10 ml ice-cold, standard electroporation buffer (10 mM potassium phosphate, pH 6.5, 50 mM sucrose). Cells were quantitated using a hemacytometer and were resuspended at a density of 10^7 cells/350 μl of standard electroporation buffer. 1 μg of plasmid cDNA library was transformed per 350 μl of cells. Transformation was performed by electroporation using a Gene Pulser (BioRad). Cells were pulsed one time in a 0.4-cm cuvette at 3 μF. The optimal field strength was determined for each cell line (2,500 to 3,250 eV/cm). After electroporation, 1 ml of ice-cold HL-5 was added to allow the cells to recover. Cells were grown for 20–24 h at 22°C in Hans' enriched HL-5, then the media was replaced with Hans' enriched HL-5 with the appropriate concentration of G418. The media was changed every 2–3 d until the clones were harvested. For the ORF+ derived strains, a lower limit of 1,500 colonies/μg of DNA was typically recovered. For this estimation, only the largest colonies were counted to prevent overestimation due to counting small, sibling satellite clones. This means that the actual number of colonies recovered per microgram of DNA might have been much greater. This conservative estimate was used for estimating the coverage of the cDNA library.

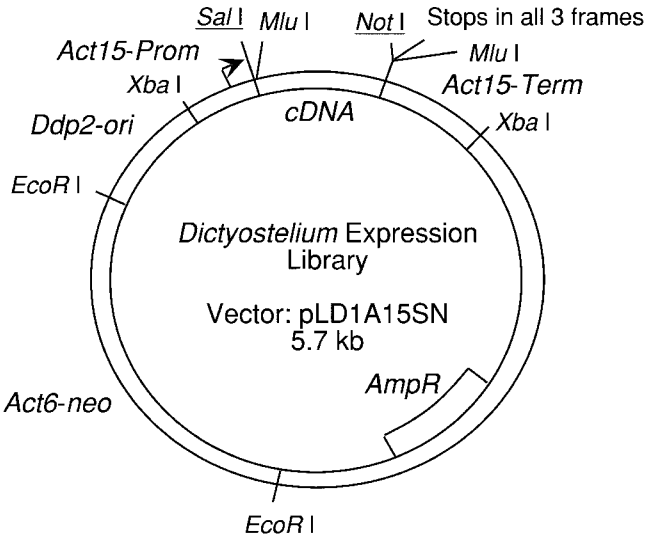

Figure 1. Map of the *D. discoideum* expression cDNA library. Underlined restriction sites are unique unless present in a given cDNA.

Selection of Suppressors

After the *D. discoideum* library clones reached near confluency on 10-cm plates, the cells were harvested and combined into eight distinct pools of 30,000–35,000 clones per pool. Therefore, a total of 240,000–280,000 independent clones were analyzed in the selection experiment. One seventh of each pool was subjected to growth selection. The aliquots of cells used for selection were grown in 100-ml cultures in 1-liter Erlenmeyer flasks at 180 rpm. The cells were grown and split every 3 to 4 d initially, and then every 6 to 7 d. Initial splits were 1 to 2, and were then 1 to 4, 1 to 6, 1 to 10, 1 to 30, 1 to 50, 1 to 100, 1 to 500, and finally 1 to 1,000. Growth rates of the cells were monitored throughout the entire selection. The pools were selected for 1.5–2.5 mo. This amount of time was required for the winners to emerge from the population since the mutant 11-5.1 cells can grow slowly in suspension culture, and since the winners had to emerge from a background of 30,000–35,000 clones. Once the cultures were being split at 1 to 1,000 every 6 to 7 d and the cell morphology appeared more wild-type, DNA was harvested using the Wizard preparation protocol (Promega). DNA was transformed into STBL2 cells (GIBCO BRL) and 18 clones were selected for alkaline lysis DNA preparation and restriction endonuclease digestion. Appropriate clones were selected and the sequence of the DNA was determined using standard procedures. Recovered clones were transformed into the original mutant cell line to verify that the DNA construct could recapitulate the suppression effect.

Growth Rate and Nuclei/Cell Ratio Determination

Relative growth rates were determined by diluting the cells to a similar starting density and measuring the cell densities over several subsequent time points with a hemacytometer. The cell densities were plotted versus time and the resulting log phase curve was fit to a single exponential equation using KaleidaGraph (Synergy Software). During the log phase of growth, aliquots of cells were removed, fixed with −10°C methanol, and washed in 1× PBS, 0.1% Triton X-100 (PBT). Alternatively, cells were fixed in 4% paraformaldehyde (Electron Microscopy Sciences) in HL-5 media for 10 min, and then for 50 min in 4% paraformaldehyde in 1× PBS, followed by 3 min in −10°C acetone. Cells were washed in 1× PBS. Cells were stained with DAPI (1 μg/ml; Molecular Probes) for 20 min with gentle rocking. After washing, the cells were examined by fluorescence microscopy using a microscope (Axiovert; ZEISS). To determine

the nuclei/cell ratios for strains grown on surfaces, cells were plated at low density (~2–5 × 10^5 cells/ml) and grown for 2 d. They were then fixed using the paraformaldehyde procedure described above. The number of nuclei per cell was recorded for a few hundred cells.

Genomic DNA Analysis

Genomic DNA was prepared from wild-type (ORF+7-3) and 11-5.1 cells. Genomic DNA was digested singly with EcoRI, HindIII, and XbaI, and doubly with HindIII/XbaI and EcoRI/XbaI restriction endonucleases. The DNAs were separated on a 1% agarose gel and depurinated, denatured, and neutralized before transferring to Hybond-N+ nylon membrane (Amersham Pharmacia Biotech) by capillary transfer using standard protocols. Immobilized DNAs were hybridized with denatured α-^{32}P–labeled DNA probes using the random hexamer extension protocol (Feinberg and Vogelstein, 1983). Hybridized fragments were detected using a PhosphoImager (Molecular Dynamics) and autoradiography. For *cortexillin I*, the 840-bp SalI/NotI cDNA insert from cortI 2A19 was used as a probe. For *dynacortin*, the SalI/NotI cDNA from a full-length *dynacortin* cDNA clone was used.

RNA Analysis

Total RNA was isolated using the TRIzol method (GIBCO BRL). RNA was quantitated using a DU 640 spectrophotometer (Beckman Coulter), separated on a 1% agarose-formaldehyde gel, and transferred to Hybond-N+ nylon membrane (Amersham Pharmacia Biotech) by capillary transfer. DNA probes were labeled as above. Immobilized RNAs were hybridized with denatured α-^{32}P–labeled DNA probes in Church's buffer (250 mM sodium phosphate, pH 7.0, 7% SDS, 1% BSA, 1 mM EDTA). Hybridized RNAs were detected by autoradiography.

Isolation of Full-length cDNAs and Sequence Analysis

Full-length cDNAs were isolated from the cDNA library described above. Colonies were plated on Luria broth agar plates, transferred to Hybond-N+ nylon membrane, and hybridized with radiolabeled probes. Plasmid DNA was isolated from the cells and the sequence of the insert was determined. Because the vector backbone is a *D. discoideum* expression vector, the full-length cDNA plasmids could be reintroduced into *D. discoideum* directly to test the in vivo function of the full-length cDNA. DNA and protein sequence analysis was performed using SeqWeb (Wisconsin Package Version 10.0, Genetics Computer Group, Madison, WI), and the Expasy Proteomics Tools web site (www.expasy.ch). BLAST searches (Altschul et al., 1997) were also conducted either through the SeqWeb interface or through the NCBI web site (www.ncbi.nlm.nih.gov).

Antibody Production and Western Analysis

The entire dynacortin 2B19 coding sequence (encoding amino acids 118–354) was expressed in *Escherichia coli* as a glutathione S-transferase (GST) fusion using the pGex-1 vector. The GST:2B19 protein was purified on glutathione resin (Sigma-Aldrich), using standard conditions. Rabbit polyclonal antibodies were generated using a standard protocol for antibody production.

For Western analysis, cell lysates were prepared by boiling cells in SDS sample buffer. Proteins were electrophoretically separated on SDS-polyacrylamide gels and transferred to nitrocellulose. The dynacortin protein was detected using the antidynacortin rabbit polyclonal antibody and a goat anti–rabbit, HRP-conjugated, secondary antibody (BioRad). The coronin protein was detected using the anticoronin mAb (deHostas et al., 1991) and a goat anti–mouse, HRP-conjugated, secondary antibody (Bio-Rad). Immune complexes were detected using the ECL detection system (Amersham Pharmacia Biotech).

Cell Fractionation

Log phase cells were recovered and washed in 10 mM Tris, pH 7.4. Cells were resuspended in lysis buffer (75 mM NaCl, 150 mM Hepes, pH 7.1, 3 mM EDTA, 2 mM EGTA, 0.1 mM PMSF, 55 μg/ml TLCK, 80 μg/ml TPCK, 2 μg/ml leupeptin, 5 μg/ml pepstatin) ± 20 mM sodium vanadate (Na_2HVO_4; referred to as NaV_i). Cells were lysed by 3 cycles of freezing in liquid N_2 and immediately thawing. Cells were centrifuged in a TLA 120.1 rotor (Beckman Coulter) at 100,000 *g* for 30 min. Supernatant and pellet fractions were analyzed by SDS-PAGE and Western analysis as described above.

For complex sizing analysis, the 100,000-*g* supernatants were prepared in a modified lysis buffer (20 mM NaCl, 150 mM Hepes, pH 7.1, 2 mM EDTA, 2 mM EGTA, 20 mM NaV_i, and the same protease inhibitor cocktail). Samples were applied to a Superdex S200 HR 10/30 column (Amersham Pharmacia Biotech) and chromatographed using an MPLC system (Waters Corp.). The running buffer used for the gel filtration column was the same buffer without the 20 mM NaV_i and the protease inhibitors.

Immunocytochemistry

For in situ localization of the endogenous dynacortin, wild-type ORF+7-3, or Ax2 *D. discoideum* cells were plated on coverslips and allowed to adhere for 4 h to overnight. Cells were either fixed in −10°C methanol for 3 min or in 4% paraformaldehyde (Electron Microscopy Sciences) in HL-5 for 10 min followed by 50 min in 4% paraformaldehyde in 1× PBS, then −10°C acetone for 3 min. Cells were blocked for 10 min in 1× PBS, 0.5% BSA (PBT). If cells were fixed in −10°C methanol, 0.05% Triton X-100 was added to the PBT. Cells were immunostained with the antidynacortin polyclonal antibodies (1:1,500) in PBT. Antibodies were detected by indirect immunofluorescence using TRITC or FITC-conjugated donkey anti–rabbit secondary antibodies (Molecular Probes) as appropriate. For nuclei staining, 4′,6′-diamidino-2-phenylindole (DAPI; Molecular Probes) was added at a concentration of 1 μg/ml and for filamentous actin staining, rhodamine-phalloidin (Sigma-Aldrich) was added at 0.1 μg/ml. All washes were also done in either 1× PBS or PBT.

Microscopy

Cell imaging was done with a 40× (NA 0.75) or a 63× objective (NA 1.3) on a microscope (Axiovert; ZEISS). Images were collected using the Metamorph Software package (Universal Imaging Corp.) and images were processed with Adobe Photoshop (Adobe Systems Inc.). Ratio imaging was performed by determining the ratio of the maximal pixel intensity of the protrusion (Max. I [protrusion]) and the maximal pixel intensity of the lateral membrane (Max. I [lateral membrane]). To determine the number of protrusions of the cell, we examined the number of protrusions present on the cell at 30-s intervals. This provides a dynamic factor and allows periodic quiescent cells to be represented. The counts were determined from a single optical section of the cells so that protrusions on the extreme dorsal surface may be missed.

Results

A Genetic Screen Generated Cytokinesis-deficient Strains

We conducted a genetic screen for cytokinesis-deficient cell lines by chemically mutagenizing cells with 4-nitroquinolone-*N*-oxide and screening plates of cells for clusters of enlarged, multinucleated cells. These clusters of cells were isolated and clones were purified. The strains were subjected to growth in suspension culture, a powerfully selective condition against cytokinesis-deficient growth. The clones were also tested for the ability to complete normal development. One cell line referred to as 11-5.1 had a strong cytokinesis defect when grown in suspension culture (Fig. 2). This strain had an increased propensity to form multinucleated cells on surfaces and formed small, abnormal sorocarps (fruiting bodies) on *Klebsiella aerogenes* lawns. We used this strain in a library complementation and multicopy suppression experiment.

Library Complementation and Multicopy Suppression Analysis Revealed Four Modifiers of 11-5.1

We used cDNA library complementation to recover genetic suppressors of the mutant cell line, 11-5.1. Pools of cDNA library-transformed 11-5.1 clones were generated and were selected for reversion to wild-type or near wild-type growth (as compared with the parental strain grown

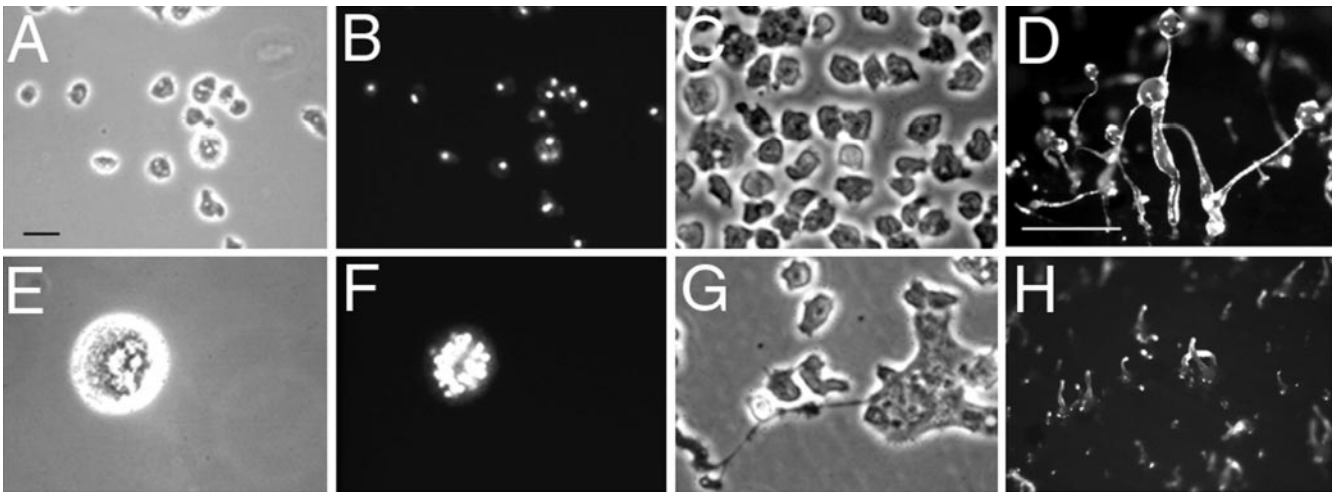

Figure 2. Phenotypic characterization of a cytokinesis-deficient mutant. A, A phase microscopy image of fixed, parental wild-type cells grown in suspension culture shows that these cells are small and uniform in size. B, DAPI staining of these wild-type cells in A reveal that the cells are largely mononucleated. C, Wild-type cells grown on surfaces are mostly small and uniform. D, Wild-type cells form large sorocarps when grown on *K. aerogenes* lawns. E, A phase microscopy image of a fixed, 11-5.1 cell grown in suspension culture shows that these cells are greatly enlarged. F, DAPI staining of the cell in E shows that it is highly multinucleated. G, 11-5.1 cells grown on surfaces have a higher proportion of enlarged cells. Long connections between the large cells and a daughter cell that is forming by traction-mediated cytofission is often observed. H, 11-5.1 cells, when plated on *K. aerogenes* lawns, form sorocarps that are reduced in size. Bars: (A–C, E–G) 10 μm; (D and H) 500 μm. Wild-type for these experiments was the ORF+7-3 strain.

under the same conditions) by growing the cells in suspension culture for several weeks. Pools were monitored for cell-doubling time, saturation density, and cell size as an indicator of the number of nuclei per cell. Periodically, aliquots of cells were also removed and grown on *K. aerogenes* lawns to screen for sorocarps with improved development. After growth in suspension culture, three pools, Tf2A, Tf2B, and Tf4C, had become near wild-type in growth rate, saturation density, and cell morphology (Fig. 3 C). DNA was isolated from these pools of *D. discoideum* and transformed into bacteria to separate individual plasmids. This step also allowed us to estimate the complexity of the *D. discoideum* strains in each pool.

Three plasmid species were recovered from Tf2A (Table II). Initially, plasmids 2A19 and 2A24 were isolated from Tf2A. Sequence analysis of these two plasmids revealed that 2A19 encoded a fragment of cortexillin I (Faix et al., 1996) and that 2A24 encoded coronin (deHostas et al., 1991) in the antisense orientation. To see whether both plasmids were in the same clone of *D. discoideum* cells, we isolated clones from the rescued Tf2A pool by plating the cells on *K. aerogenes* lawns and picking discrete plaques. We grew up several discrete clones and isolated DNA to examine the plasmid content. Indeed, both 2A19 and 2A24 were found in the same clone of cells. However, a third plasmid, 2A5, was discovered in a separate clone. 2A5 also encoded a version of the *cortexillin I* cDNA. The 2A19 and 2A5 isolates were distinct from one another since the cDNA insert sizes and the 5′ ends were different. They were predicted to encode versions of the cortexillin I that are missing most of the NH_2-terminal actin binding domain, but did include the coiled-coil domain and the COOH-terminal domain. These three plasmids are now referred to as cortI 2A19, cortI 2A5, and coroninAS 2A24. Furthermore, the *D. discoideum* clones that contained both *cortexillin I* (cortI 2A19) and the *coronin* antisense plasmid (coroninAS 2A24) developed more slowly, probably as a result of a phagocytosis defect (Maniak et al., 1995) induced by the *coronin* antisense construct. The cells expressing cortI 2A5 had no obvious developmental defect. The *coronin* antisense construct, coroninAS 2A24, was surprising in two ways. First, the library was constructed to express the inserts in the sense orientation. However, the *coronin* antisense cDNA could have primed from the 5′ untranslated region, which might be possible due to the high AT content of noncoding sequences in *D. discoideum*. Second, coronin (deHostas et al., 1993) and cortexillin I (Faix et al., 1996) are known proteins involved in cytokinesis and the likelihood of coronin and cortexillin constructs randomly appearing in the same *D. discoideum* cell is highly unlikely. For example, if one were to estimate 7,000 vegetatively expressed genes each equally represented, then the probability is $\sim 2 \times 10^{-8}$. This is probably a lower limit estimation since all genes are not represented equally.

Three plasmid species (2B7, 2B19, and 2B25; Table II) were recovered from Tf2B and one plasmid species (4C2) was recovered from Tf4C. DNA sequence analysis revealed that two of these plasmids (2B19 and 4C2) encoded the same protein that has unknown function and that we named dynacortin based on its cellular distribution (see below). 2B19 and 4C2 represent independent isolates since they were recovered from separate pools and since DNA sequence analysis revealed that the cDNA inserts began at slightly different points at the 5′ end. 2B25 encodes an ezrin-radixin-moesin (ERM)-family protein, which will be described elsewhere. Periodically, aliquots of cells were removed from each pool and plated on *K. aerogenes* lawns

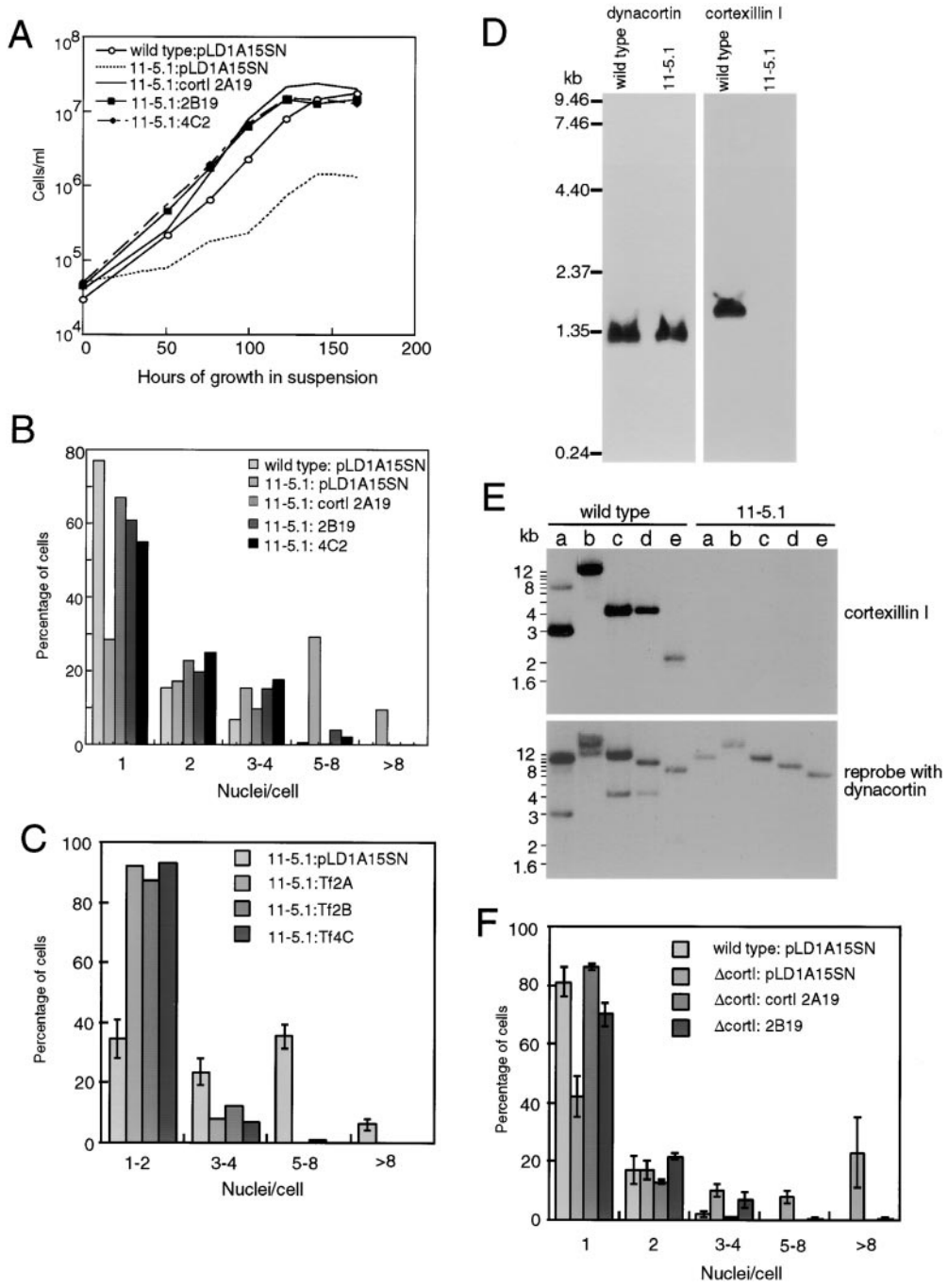

Figure 3. Characterization of rescue of 11-5.1's growth in suspension by cortI 2A19, 2B19, and 4C2. A, Introduction of these plasmids into fresh 11-5.1 cells allows rescue of the growth rates and saturation densities of these cells compared with 11-5.1 transformed with pLD1-A15SN with no insert. The wild-type and 11-5.1 control cells carried the parental vector, pLD1A15SN, with no insert. A compilation of growth experimental data is shown in Table III. B, Analysis of the distributions of the number of nuclei/cell for each strain shows that cortI 2A19, 2B19, and 4C2 dramatically improves the distribution of nuclei/cell, increasing the number of mononucleated cells. Number of cells counted for each genotype was as follows: wild-type:pLD1A15SN, 175; 11-5.1:pLD1A15SN, 271; 11-5.1:cortI 2A19, 215; 11-5.1: 2B19, 197; 11-5.1:4C2, 272. In other growth experiments, the cellular morphology, which is an effective indicator of the nuclei/cell distribution, was clearly rescued as determined by viewing the cells in the microscope. C, For comparison, the nuclei/cell distributions of cells grown in suspension from the rescued pools Tf2A, Tf2B, and Tf4C cells are shown. Data acquired from 11-5.1 cells transformed with pLD1A15SN and from pools Tf2A and Tf4C before the selection process were pooled to calculate SEM (bars) for the unrescued 11-5.1 mutant strain grown in suspension culture (11-5.1:pLD1A15SN in the histogram). The sizes of the data sets were $n = 271$, 132, and 124 cells, respectively. 11-5.1:Tf2A, 11-5.1:Tf2B, and 11-5.1:Tf4C were pools Tf2A, Tf2B, and Tf4C after the selection process. The data sets were based on $n = 60$, 92, and 108 cells, respectively. D, 2B19 recognized a 1.2-kb transcript that is present in both wild-type and 11-5.1 cells. The expected 1.4-kb *cortexillin I* transcript was found in wild-type, but was undetectable in 11-5.1 cells. This experiment is representative of three independent experiments using three independent preparations of RNA. E, Analysis of restriction endonuclease-digested wild-type and 11-5.1 genomic DNA revealed that most or all of the *cortexillin I* locus is absent in 11-5.1 cells. The immobilized, electrophoretically separated DNAs were hybridized first with a *cortexillin I* cDNA probe and were then reprobed with a *dynacortin* cDNA probe. The fragments detected with the *cortexillin I* probe are still visible after reprobing with the *dynacortin* cDNA probe. a, EcoRI digest; b, HindIII digest; c, XbaI digest, d, HindIII/XbaI double digest; e, EcoRI/XbaI double digest. 8–9 μg of genomic DNA per lane. F, Analysis of the nuclei/cell distribution of Δ*cortI* cells transformed with pLD1A15SN, cortI 2A19, or 2B19 revealed that cortexillin I and dynacortin 2B19 suppressed this mutant. These cells were grown in standard HL-5 media. Presented are the mean and SEM from three to four data sets per line, where each data set typically included 100–300 cells. Wild-type for experiments in A–E was the parental ORF+7-3 strain. Wild-type for the experiment in F was the parental line, Ax2-214.

Table II. Summary of Constructs Analyzed

Construct	Protein encoded	How generated	Rescue/suppression results			
			ORF+7-3	*cortI*$^{11\text{-}5.1}$	*myo II*$^-$	*RacE*
pLD1A15SN	None	Construction	Control	Control	Control	Control
pLD1A15:cortI 2A19	Cortexillin I (aa 208–444)	Selection	No effect	Rescues	No effect	No effect
pLD1A15:cortI 2A5	Cortexillin I (aa 179–444)	Selection		Rescues		
pLD1A15:cortI 2B7	Cortexillin I (aa 179–444)	Selection		Rescues development		
pLD1A15:dynacortin 2B19	Dynacortin (aa 173–354)	Selection	No effect	Rescues	No effect	No effect
pLD1A15:dynacortin 4C2	Dynacortin (aa 173–354)	Selection	No effect	Rescues	No effect	No effect
pLD1A15:dynacortin	Dynacortin (aa 1–354)	Library hybridization screen	DD	DD	DD	No effect
pLD1A15:GFP-dynacortin	GFP fused to the NH_2 terminus of dynacortin	Construction				
pLD1A15:coroninAS 2A24	Antisense *coronin* transcript	Selection	*coron*$^-$	*coron*$^-$	*coron*$^-$ on surfaces; larger than *myo II*$^-$ in suspension	NT
pLD1A15:coronin-GFP	GFP fused to the COOH terminus of coronin	Construction	Increases growth rate	Increases cell size in suspension and surfaces	No effect	No effect
pLD1A15:RacE	RacE	Construction	No effect	No effect	DD	Rescues
pLD1A15:GFP-myosin II	myo II heavy chain	Construction	No effect	No effect	Rescues	NT

NT, Not tested; DD, dominant cytokinesis defect.

to assay for development. The 2B7 plasmid was isolated from a rescued clone of cells exhibiting normal sorocarp morphology. 2B7 also encoded a version of cortexillin I that lacked most of the NH_2-terminal actin binding domain.

To verify that the reversion in the rescued lines is due to the plasmid isolated from the cells, the plasmids, cortI 2A19, cortI 2A5, 2B19, and 4C2, were transformed into fresh 11-5.1 cells (Fig. 3, A and B; Table II). Both cortI 2A19 and cortI 2A5 rescued 11-5.1's growth in suspension, including growth rate, saturation density, and cell morphology (Fig. 3, A and B; Table III). 2B19 and 4C2 also rescued 11-5.1's growth in suspension according to all of the criteria used (Fig. 3, A and B; Table III). Rescue by all of these constructs was apparent within a few days after being placed under suspension growth conditions and they rescued immediately after introduction into fresh 11-5.1 cells. In other words, long periods of selection were not required for rescue by the plasmids upon reintroduction into 11-5.1. The *coronin* antisense construct, coronAS 24, when introduced by itself, did not rescue 11-5.1, but instead induced a strong *coronin*$^-$ phenotype (deHostas et al., 1993) in wild-type, 11-5.1, and myo II heavy chain (*myo II*$^-$) mutant cells (Table II).

From the average growth rate of 11-5.1:pLD1A15SN ($k = 0.019 \pm 0.002\ h^{-1}$), the amount of time required for one rescued cell to emerge from a background of 35,000 mutant cells (a typical background size in the selection experiment) can be estimated. For example, a cell such as 11-5.1:2B19 with a relative growth rate of 1.7 ($k = 0.032\ h^{-1}$; Table III) would be expected to reach 100-fold excess over the mutant background in 6.9 wk. This is in good agreement with the 8.5 wk required for 11-5.1:2B19 to emerge as a winner. In contrast, an 11-5.1:cortI 2A19 cell with a relative growth rate of 2.1 ($k = 0.039\ h^{-1}$; Table III) would be expected to reach 100-fold excess in only 4.4 wk. In fact, the *cortexillin I* winners were recovered in 6.5 wk. Since other factors besides log phase growth contribute to the total culture time, it is not surprising that the observed time would be a little longer than the theoretical time.

Intriguingly, the list of plasmids described above were the only plasmids recovered from rescued pools with one exception. One clone of *discoidin Ic* (Devine et al., 1981) was recovered from a fourth pool, Tf4D, using the developmental assay. Reintroduction of the plasmid was able to rescue the development of the 11-5.1 cells when plated at high density, but not low density (plated for single discrete plaques). It did not, however, rescue growth in suspension

Table III. Cortexillin I 2A19 and 2B19/4C2 Constructs Increase the Growth Rates and Saturation Density of 11-5.1 Cells Grown in Suspension

Strain	Relative growth rate, *k*	R	Fold increase of final saturation density
	Mean ± SEM	*Mean ± SEM (n)*	*Mean ± SEM (n)*
Wild-type:pLD1A15SN	1.8 ± 0.2	0.98 ± 0.01 (5)	8.9 ± 1.1 (5)
11-5.1:pLD1A15SN	[1]	0.94 ± 0.02 (18)	[1] (18)
11-5.1:cortI 2A19	2.1 ± 0.1	0.99 ± 0.003 (16)	11 ± 1.3 (17)
11-5.1:2B19	1.7 ± 0.1	0.99 ± 0.001 (9)	7.6 ± 1.0 (16)
11-5.1:4C2	2.0	0.99 (1)	7.5 ± 0.2 (2)

The relative growth rate and final saturation densities were normalized to 11-5.1:pLD1A15SN, which was used as the reference for each experiment. The 11-5.1:pLD1A15SN normalized data are bracketed to note that fact. For the relative growth rates, cell densities from the log phase of growth were plotted against time and were fitted to an exponential equation. R values are the correlation coefficients from each curve fit. This is a measure of how well a particular strain's log growth phase fit to an exponential equation. Differences between the rescued strains and the 11-5.1:pLD1A15SN strain for growth rate and R values were significant (one-tailed *t* test: $P < 0.0005$). Differences in saturation density were also significant (one-tailed *t* test: $P < 0.00005$). *n*, Experiments used to calculate each parameter. Data were compiled from seven independent transformations of fresh 11-5.1 cells with pLD1A15SN, cortI 2A19, and 2B19. Wild-type was transformed three times and 4C2 was transformed into 11-5.1 once for this data set. An example of one experiment is shown in Fig. 3 A. Wild-type is the ORF+7-3 strain. Cells were grown in 15 μg/ml G418 in Hans' enriched HL-5 media, and multiple lots of media were used over the course of all of the experiments, which likely account for much of the variation.

in the original transformant or when reintroduced into fresh 11-5.1 cells. It was not studied further.

Examination of mRNAs and Genomic DNA Indicates 11-5.1 Is an Allele of Cortexillin I

To determine which of the genes was mutated in 11-5.1, we began by examining the mRNA levels of each of the genes in 11-5.1 cells compared with the parental strain (Fig. 3 D). Since the *cortexillin I* constructs and the 2B19/4C2 constructs rescued 11-5.1's growth in suspension to wild-type levels, we began examining these two genes first. The 1.4-kb *cortexillin I* mRNA was completely absent in 11-5.1 cells, but present in the parental wild-type cells. The 1.2-kb 2B19/4C2 mRNA was present in both strains. In addition, hybridization of restriction-digested genomic DNA with a *cortexillin I* cDNA probe revealed that the majority of the *cortexillin I* locus is absent in the 11-5.1 strain, whereas the *dynacortin* locus appeared to be normal in both strains (Fig. 3 E). Since we were able to rescue all of the defects (growth in suspension and development) of 11-5.1 with *cortexillin I* constructs and all or most of the *cortexillin I* genomic locus and its transcript are absent in 11-5.1, 11-5.1 is an allele of *cortexillin I*. Strain 11-5.1 will be referred to as $cortI^{11\text{-}5.1}$.

Dynacortin 2B19 Suppresses an Independent Allele of cortexillin I

To test whether cortI 2A19 and dynacortin 2B19 could complement an independent *cortexillin I* mutant cell line, both constructs were transformed into an Ax2-derived strain in which the *cortexillin I* locus had been deleted by homologous recombination (Δ*cortI*; Faix et al., 1996). Both plasmids rescued Δ*cortI* cells; however, the 2B19 plasmid offered a modest, but significant, rescue of the growth properties of this strain when the cells were grown in Hans' enriched HL-5 media (Table IV). Both plasmids rescued to a higher level when the cells were grown in standard HL-5 media (Fig. 3 F, Table IV). The differences in the growth properties of the Δ*cortI* cells under the two media conditions suggest that these cells are more sensitive to environmental conditions; it will be useful to determine whether that is a general property of cytokinesis-impaired strains. Furthermore, since dynacortin 2B19 suppressed this strain, it indicates that its suppression of the loss of *cortexillin I* is general and not specific to a particular genetic background.

The Dynacortin Gene Encodes a Novel, Serine-rich Protein

The cDNA insert in 2B19 was only ~720 bp, whereas the transcript detected by mRNA blot analysis was ~1.2 kb. We isolated and sequenced two full-length clones from the cDNA library described in this paper. The ORF in the *dynacortin* cDNA predicts a protein of 354 amino acids with a calculated molecular weight of 37.9×10^3 M_r and a predicted pI of 7.32 (Fig. 4). The protein contains 65 serines, 29 threonines, and 6 tyrosines (28.4% hydroxyamino acids). A candidate PEST sequence (Rogers et al., 1986) that extends from residues 61–91 and an α-helical hydrophobic stretch at the very COOH terminus extending from residues 336–354 were identified. There are also several candidate phosphorylation sites. BLAST searches (Altschul et al., 1997) using the protein predicted from the full-length transcript identified no definitive homologues in other organisms. However, it did identify some distantly related molecules. One protein was a putative 113-kD membrane protein (Ymr317wp) from *Saccharomyces cerevisiae*. Pairwise alignments between the two proteins showed homology over 365 amino acids at the level of 36% identity and 40% similarity with 24 relatively small gaps. One *C. elegans* ORF (zc47.3b) also was identified as a related protein by BLAST searching and had a similar level of homology. We used a large number of other available sequence analysis algorithms, none of which revealed any additional informative similarities. Finally, due to the low quality scores and the large number of gaps in each of the pairwise alignments, we concluded that the similarities are unreli-

Table IV. Rescue of a cortexillin I Deletion Strain by cortI 2A19 and dynacortin 2B19

Strain	Relative growth rate, *k*	R	Fold increase of final saturation density
	Mean ± SEM	*Mean ± SEM (n)*	*Mean ± SEM (n)*
Hans' enriched HL-5 media			
Wild-type:control plasmid	2.4 ± 0.3	0.99 ± 0.004 (4)	9.5 ± 2 (5)
Δ*cortI*:control plasmid	[1]	0.92 ± 0.03 (4)	[1] (5)
Δ*cortI*:cortI 2A19	1.8 ± 0.1	0.99 (2)	5.6 ± 0.3 (4)
Δ*cortI*:2B19	1.6 ± 0.09	0.99 ± 0.007 (4)	2.8 ± 0.3 (5)
Standard HL-5 media			
Wild-type:pLD1A15SN	207 ± 0.4	0.99 ± 0.005 (3)	8.3 ± 0.4 (3)
Δ*cortI*:pLD1A15SN	[1]	0.95 ± 0.009 (8)	[1] (8)
Δ*cortI*:cortI 2A19	2.1 ± 0.08	0.98 ± 0.008 (8)	5.5 ± 0.3 (8)
Δ*cortI*:2B19	2.2 ± 0.2	0.98 ± 0.007 (8)	3.8 ± 0.3 (8)

Data were collected and analyzed as in Table III. Analysis indicates media conditions affect the ability of the Δ*cortI* stain to grow. Data were compiled for two independent transformations for cortI 2A19 pLD1A15SN and 2B19 pLD1A15SN. Since the Δ*cortI* was generated with the G418-resistance marker, cortI 2A19 and 2B19 pLD1A15SN had to be transformed with a cocktail of plasmids that included a blasticidin resistance plasmid to select for cells that acquired DNA. Cells were then grown in suspension culture to select for rescue. Both plasmids showed rescue with identical time courses. Data of growth of cells in Hans' enriched HL-5 media also includes results from cells transformed with a 2B19 expression construct that contains a blasticidin resistance marker. The appropriate vector backbone was transformed into the wild-type and Δ*cortI* cells (denoted control plasmid). Comparisons were only made between cells with the appropriate control plasmid. Only cells carrying the pLD1A15SN-derived plasmids were assayed in standard HL-5 media. For cells grown in standard HL-5 media, differences in all growth parameters were significant for wild-type and rescued strains compared to the mutant (one-tailed *t* test: growth rate, $P < 0.00005$; R value, $0.01 < P < 0.025$; and saturation density, $P < 0.00005$). The wild-type strain for these experiments was the Ax2-214 strain.

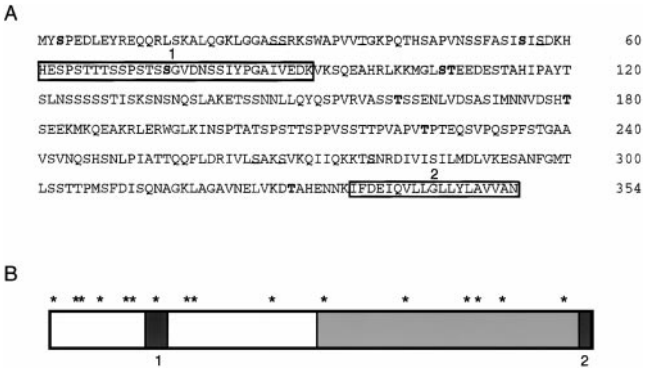

Figure 4. Sequence features of dynacortin. A, The *dynacortin* gene encodes a protein that has high serine and threonine content. There are also multiple consensus phosphorylation sites. Consensus casein kinase II sites are in bold, consensus protein kinase C sites are underlined, and the only consensus protein kinase A site is italicized. Box 1 encloses a candidate PEST sequence, which has a PEST search score of 12.34 (Rogers et al., 1986). Box 2 encloses an α-helical, hydrophobic patch at the COOH terminus. B, A cartoon of the linear relationship between the PEST sequence, the COOH-terminal hydrophobic patch, and the phosphorylation sites (asterisks) is presented. The region encoded by dynacortin 2B19 (amino acids 173–354) is shown as a gray box. The dynacortin sequence is available (GenBank/EMBL/DDBJ accession number AF222688).

able, and the biochemical function of this protein will have to be discerned experimentally.

Dynacortin Is a Soluble Protein and Part of a Larger Complex

With the hydrophobic stretch at the COOH terminus and the low similarity with the putative membrane associated protein, we speculated that dynacortin may be a membrane-associated protein. To test this, we generated rabbit polyclonal antibodies against the 237 amino acids encoded by the 2B19 portion of dynacortin and examined the partitioning of the protein during cell fractionation (Fig. 5 A). Native cell lysates were prepared, and the lysates were subjected to high speed centrifugation. The dynacortin protein partitioned into the soluble fraction; however, it had a lower apparent molecular weight than that observed in whole cell lysates prepared by boiling in SDS-sample buffer. This mobility shift was inhibited by adding 20 mM sodium vanadate to the lysate. The mobility shift does not seem to be due to phosphotyrosines. Lower concentrations of sodium vanadate were less effective at inhibiting the mobility shift and antiphosphotyrosine antibodies did not detect immunoprecipitated dynacortin (data not shown). In addition, preliminary results indicate that ^{32}P-labeled dynacortin can be immunoprecipitated from extracts prepared from metabolically labeled cells (data not shown). Numerous other conditions were also tested and the protein always partitioned into the supernatant fraction (data not shown). In summary, these data are consistent with the protein being a soluble phosphoprotein and if it associates with the membrane, it does so with low affinity.

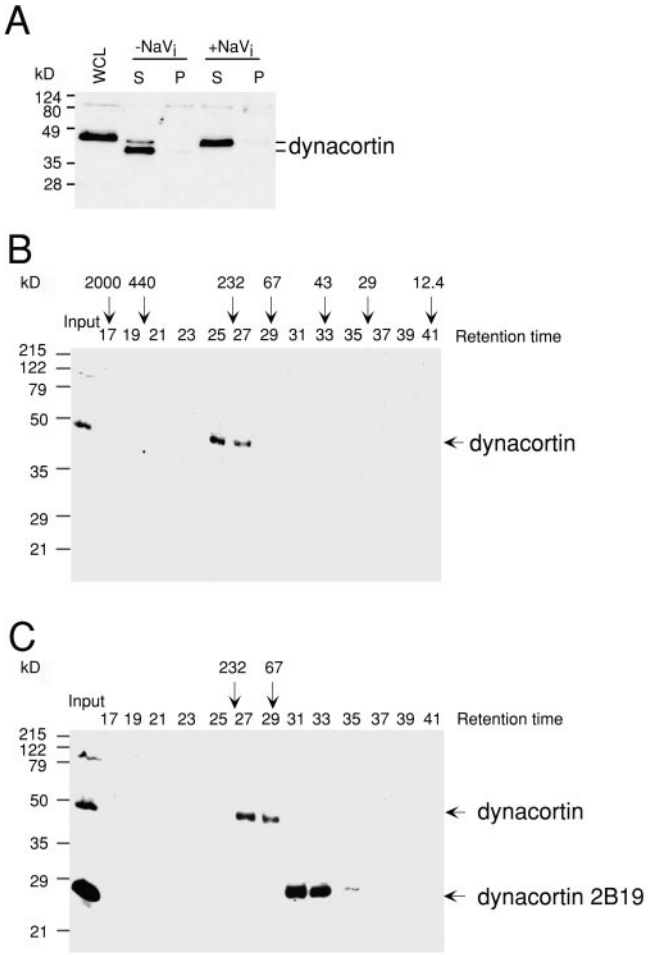

Figure 5. Dynacortin is a soluble protein that forms a high molecular weight complex. A, Dynacortin is a soluble protein that might contain phosphates. Western analysis of cell lysates prepared by boiling in SDS-PAGE sample buffer (WCL) reveals a protein with an apparent molecular weight of ~48 kD. Dynacortin partitions into the 100,000-*g* supernatant, but has a faster mobility more similar to the expected 38-kD mol wt calculated from the primary sequence when the cell lysates are prepared in the absence of sodium vanadate ($-NaV_i$ lanes). The addition of 20 mM sodium vanadate ($+NaV_i$), an inhibitor of phosphatases, blocks this mobility shift, suggesting that the mobility shift is due to dephosphorylation of the protein upon cell lysis. The dynacortin species in the WCL lane and the dynacortin species in the $+NaV_i$ supernatant lane comigrate when mixed, verifying that these are the same molecular weight forms (not shown). S, 100,000-*g* supernatant; P, 100,000-*g* pellet. B, The wild-type soluble dynacortin complex migrates on a gel filtration column comparable to a globular 250–300-kD complex. The supernatant analyzed in B was prepared from native 100,000-*g* supernatants from wild-type ORF+7-3 cells carrying the pLD1A15SN plasmid with no insert. C, The wild-type complex is disrupted by the expression of the dynacortin 2B19 version. The complex molecular weight is ~100 kD smaller, and the 2B19 version is ~50 kD, larger than expected for the 20-kD monomer, suggesting that it may be titrating out a cofactor. The supernatant analyzed in C was prepared from native 100,000-*g* supernatants from ORF+7-3 cells expressing dynacortin 2B19. Retention time in B and C is in minutes.

We then examined whether dynacortin was associated with higher molecular weight complexes in the cell by applying the high speed supernatants to a gel filtration column. In wild-type cells, the protein had a retention time comparable with a globular complex of 250-300 kD in size (Fig. 5 B). In wild-type cells expressing the dynacortin 2B19 suppressor protein, the molecular weight of the endogenous dynacortin was downshifted by ~100 kD (Fig. 5 C). In addition, on the gel filtration column, the retention time of the 2B19 version was comparable to a globular protein of 50 kD, which is larger than expected for a globular, monomeric 182 amino acid protein. Dynacortin 2B19 construct encodes the COOH 237 amino acids of dynacortin; however, only the COOH-terminal 182 amino acids are expected to be translated due to the position of the most 5′ ATG. Indeed, a construct that encodes only the COOH-terminal 182 amino acids produced a comparably sized protein as the 2B19 construct (data not shown). The retention times on the gel filtration column of the endogenous dynacortin and the 2B19 version in Fig. 5, B and C, are consistent with the notion that the dynacortin 2B19 protein disrupts the endogenous macromolecular dynacortin complex. Purification and characterization of the native dynacortin complex is required to determine whether the dynacortin complex is homomeric or heteromeric.

We also tested for dynacortin complex formation in *cortI*$^{11\text{-}5.1}$ cells and Δ*RacE* cells and in both cases the protein complex had the wild-type retention time (data not shown). In other cell fractionation experiments, we observed that dynacortin and coronin fractionated separately even though the core dynacortin complex remained assembled (data not shown). Therefore, RacE, cortexillin I, and coronin are not likely to be present in the dynacortin core complex.

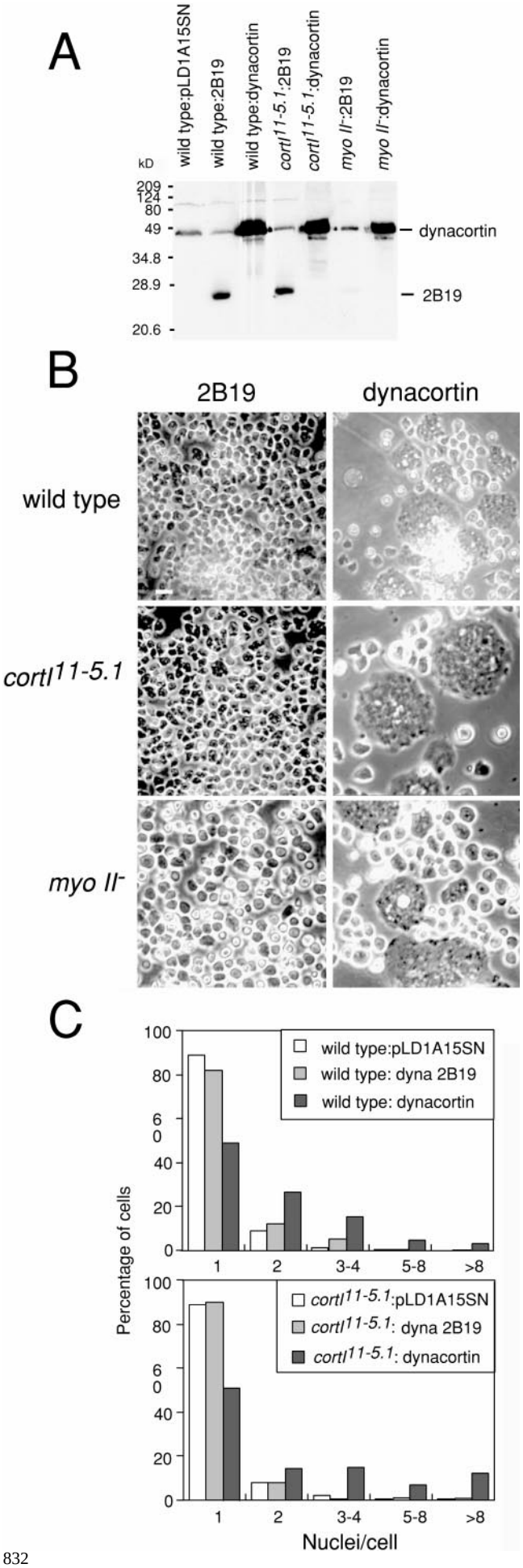

Figure 6. Dynacortin induces a dominant cytokinesis defect when overexpressed. A, Western analysis of full-length dynacortin and dynacortin 2B19 proteins in the different cell lines reveals that appropriate sized proteins are indeed expressed and that full-length dynacortin is overexpressed in each of the cell lines. Dynacortin 2B19 is easily detected in *myo II*$^-$ cells with slightly longer exposure times (not shown). B, Expression of dynacortin 2B19 in wild-type, *cortI*$^{11\text{-}5.1}$, and *myo II*$^-$ cells does not induce any deleterious effect. Overexpression of the full-length version of dynacortin in wild-type, *cortI*$^{11\text{-}5.1}$, and *myo II*$^-$ cells induces a dominant cytokinesis defect as indicated by the large, multinucleated cells when grown on surfaces. Bar, 10 μm (applies to all panels). C, The overexpression defect was quantitated by determining the distribution of cells containing each number of nuclei per cell revealed by DAPI staining. Since the growth on surfaces is a more permissive growth condition, the defect caused by the full-length dynacortin is severe. Overexpression of dynacortin in these strains caused this defect in all (three or more independent transformations for each strain) experiments. The following number of cells were counted for each genotype for the data set presented: wild-type:pLD1A15SN, 288; wild-type:dyna 2B19, 300; wild-type:dynacortin, 374; *cortI*$^{11\text{-}5.1}$:pLD1A15SN, 289; *cortI*$^{11\text{-}5.1}$:dyna 2B19, 234; *cortI*$^{11\text{-}5.1}$: dynacortin, 192. Wild-type for these experiments was the ORF+7-3 strain.

Overexpression of Dynacortin Induces a Cytokinesis Defect

We introduced the full-length dynacortin gene into wild-type cells, *cortI*$^{11\text{-}5.1}$ cells, and *myo II*$^{-}$ cells. In all of the strains, expression of full-length dynacortin induced a prominent cytokinesis defect when the cells were grown on surfaces (Fig. 6). Interestingly, the cells sensitive to overexpression of dynacortin could overcome this defect after several weeks in culture, even though they still overexpressed the protein (data not shown). 2B19, on the other hand, did not induce a dominant defect in cytokinesis. The full-length version of dynacortin failed to rescue the growth in suspension of *cortI*$^{11\text{-}5.1}$ cells even after growing the cells in suspension for a few weeks (a period of time much longer than required for cortI 2A19 and dynacortin 2B19 to rescue *cortI*$^{11\text{-}5.1}$) to select for rescued subclones. This indicates that suppression of *cortI*$^{11\text{-}5.1}$ is specific to the dynacortin 2B19 fragment (data not shown). This fact, combined with the result that dynacortin 2B19 disrupted the endogenous dynacortin complex, suggests that dynacortin 2B19 might antagonize the wild-type dynacortin pathway to suppress the loss of cortexillin I. We verified the expression of full-length dynacortin and the 2B19 domains by Western analysis on total cell protein lysates from each cell line (Fig. 6 A). Full-length dynacortin was overexpressed relative to the endogenous protein in all of the strains examined. The dynacortin 2B19 construct also produced a protein that was overexpressed relative to the endogenous dynacortin.

Overexpression of dynacortin in *RacE* mutant cells failed to produce a cytokinesis defect (data not shown). However, overexpression of dynacortin in the parental wild-type (DH1) strain from which the *RacE* mutant cells were derived produced a defect only transiently; therefore, it is not possible to determine whether RacE is required for this defect (data not shown). This demonstrates that strain differences can affect how the cells respond to different perturbations. It is essential, therefore, to use the appropriate reference strain for phenotypic comparisons.

Dynacortin Is Enriched in Dynamic Domains of the Cell Cortex

We used the dynacortin polyclonal antibodies to identify the cellular localization of endogenous dynacortin by immunocytochemistry (Fig. 7, A and B). Dynacortin localized to the cortex and was found to be enriched at dynamic domains of the cortex, including pseudopodia (shown in

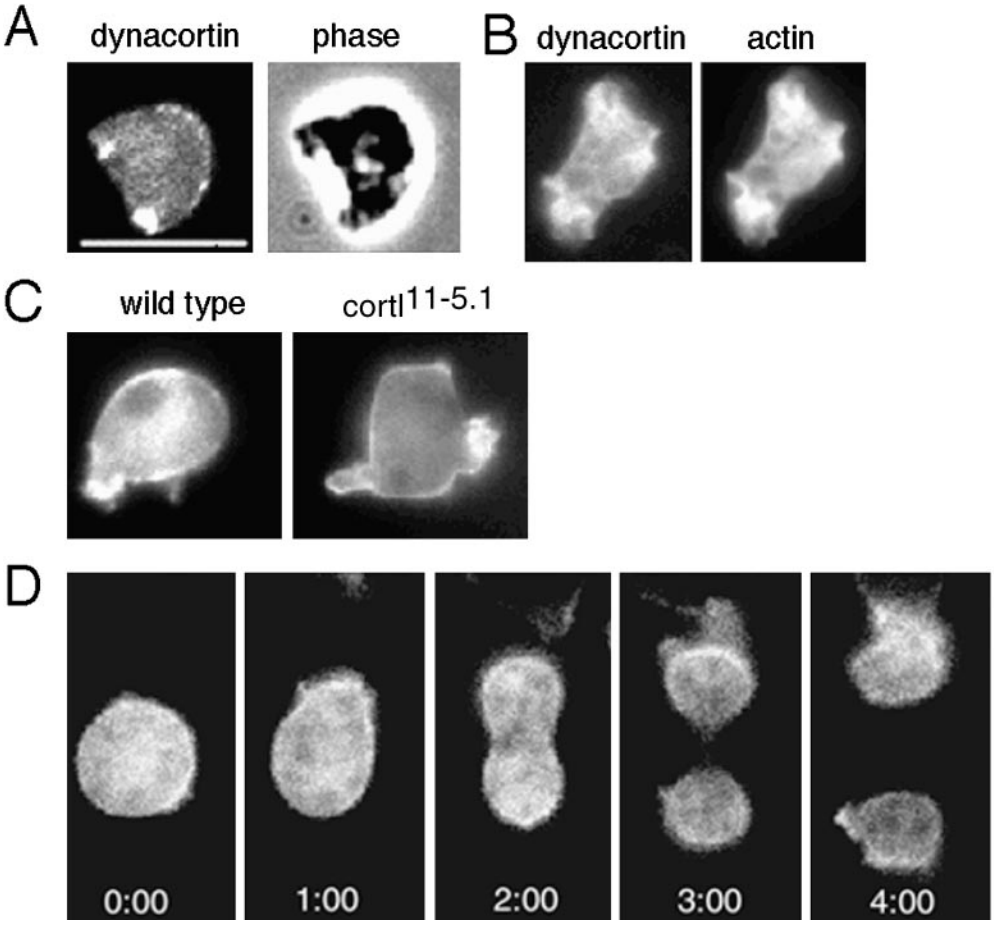

Figure 7. Localization of dynacortin. A, An immunofluorescence micrograph and a phase image of a wild-type *D. discoideum* cell reveals that endogenous dynacortin is found in the cytoplasm, is localized to the cell cortex, and is enriched at dynamic domains such as pseudopodia. This cell was fixed using the methanol procedure. B, Actin and dynacortin are coenriched in regions of cortical protrusive activity. These cells were fixed using the paraformaldehyde/acetone procedure. It should be noted that the optimal fixation conditions for preserving dynacortin are incompatible with the optimal fixation conditions for actin. The cells in Fig. 7 B were fixed under conditions that best preserve both proteins simultaneously. C, GFP-dynacortin localizes similarly to the endogenous dynacortin detected by immunocytochemistry. In both wild-type and *cortI*$^{11\text{-}5.1}$ cells, dynacortin is found at the cortex, but is enriched in protrusions. D, GFP-dynacortin is found in the cytoplasm and is evenly distributed around the cell cortex during early cytokinesis. It becomes enriched in the polar ruffles during late cytokinesis. After separation of the two daughter cells, it immediately becomes enriched in cell protrusions (4:00). Cells in C and D are imaged alive and are expressing GFP-dynacortin. Time is in minutes:seconds. Bar, 10 μm (applies to A–D). Wild-type cells in A and C are the ORF+7-3 cell line, and the cells in B are the Ax2-214 cell line. The wild-type cell in D is derived from the DH1 strain.

Fig. 7 A), filopodia, lamellipodia, and macropinocytotic crowns. A population of dynacortin can also be detected in the cytoplasm. Hence, we named the protein dynacortin for its enrichment at dynamic cortical domains. Regions of the cell cortex that were enriched for dynacortin were also enriched for filamentous actin as expected (Fig. 7 B). We also examined dynacortin localization by expressing a GFP-dynacortin fusion protein. In addition to an apparent cytoplasmic component, GFP-dynacortin localized predominantly to the cell cortex and was enriched in protrusions in wild-type and in *cortI*$^{11\text{-}5.1}$ cells (Fig. 7 C). Immunodetection of dynacortin in wild-type cells expressing dynacortin 2B19 revealed a comparable dynacortin distribution, except more abundant due to the extra protein, suggesting that the dynacortin 2B19 protein localizes similarly to the endogenous protein (data not shown).

During cytokinesis, detection of endogenous dynacortin and GFP-dynacortin was more difficult than during interphase. This suggests dynacortin might be somewhat downregulated during cytokinesis. However, GFP-dynacortin was localized globally in the cell cortex and cytoplasm and was enriched in the polar cortex. It was also reduced in the cleavage furrow and midbody during late cytokinesis (Fig. 7 D). It was enriched in the dynamic polar ruffles and immediately resumed its enrichment in protrusive domains after the completion of cytokinesis. Endogenous dynacortin revealed by immunocytochemistry had a similar distribution during cytokinesis (data not shown).

Coronin Is Not Required for Dynacortin Localization

Because we recovered a *coronin* antisense construct in one of the suppressed strains and because coronin and dynacortin are distributed similarly in the cell cortex, we examined the relationship between coronin and dynacortin. Coronin protein expression was disrupted in wild-type cells expressing the *coronin* antisense construct (Fig. 8 A). This produced a *coronin*$^-$ phenotype in these cells (Table II; deHostas et al., 1993). Interestingly, dynacortin, actin, and coronin all had identical cortical distributions (Fig. 8 B). Immunocytochemistry on cells expressing the *coronin* antisense transcript revealed that dynacortin and fila-

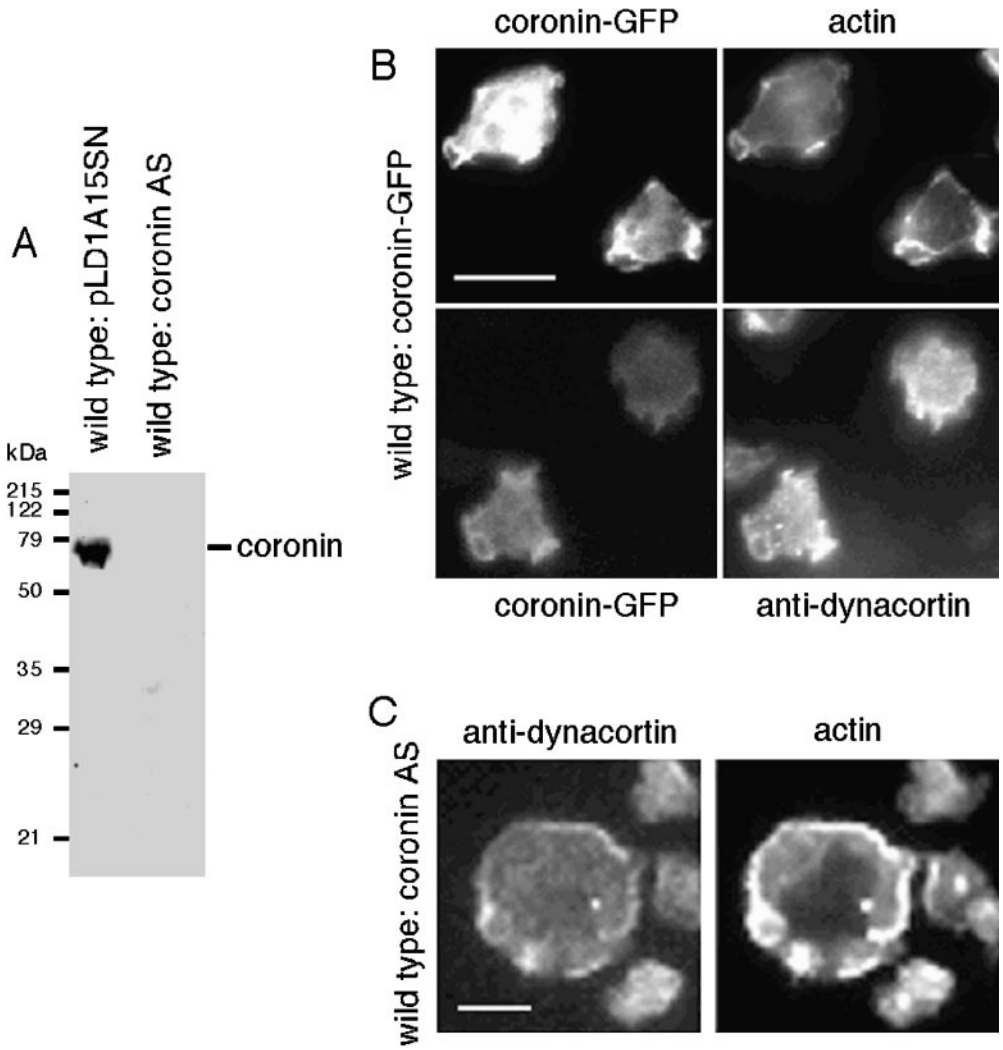

Figure 8. Coronin antisense and coronin dependence. A, The *coronin* antisense construct completely inhibits accumulation of coronin protein as determined by SDS-PAGE and Western immunodetection using anticoronin antibodies. To verify loading, protein extracts were quantitated using the BioRad protein assay and equivalent aliquots from the same samples were examined in parallel by Coomassie staining of SDS-PAGE gels and by immunodetection with antidynacortin antibodies (not shown). A similar analysis was repeated on separate protein extract preparations. B, Coronin-GFP localized to protrusive domains of the cell cortex that were also enriched for actin and dynacortin. C, Dynacortin and actin localized to the cell cortex of *coronin* antisense expressing cells. Coronin-GFP or *coronin* antisense expressing cells were fixed and stained with rhodamine-labeled phalloidin to identify filamentous actin or with antidynacortin antibodies to reveal dynacortin. Bars, 10 μm (each applies to all panels of its respective group). Wild-type for these experiments was the ORF+ 7-3 strain. These cells in B and C were fixed using the paraformaldehyde/acetone procedure.

mentous actin localized to the cell cortex and to cortical protrusions, indicating that coronin is not required for the localization of dynacortin to the actin-rich cortex (Fig. 8 C).

Dynacortin Localization Is Altered in RacE Mutant Cells

Since RacE and dynacortin are distributed similarly in the cell cortex, we examined whether RacE is required for normal dynacortin cortical distribution. In the parental wild-type (DH1) cells, GFP-dynacortin localized to the cortex and was enriched in protrusions (Fig. 9 A). In the *RacE* mutant cell lines, GFP-dynacortin appeared to be absent from the cortex between protrusions and was highly concentrated in cortical protrusions (Fig. 9 B). Coronin-GFP localization was affected similarly by the loss of RacE (Fig. 9 C). To quantify these observations, we

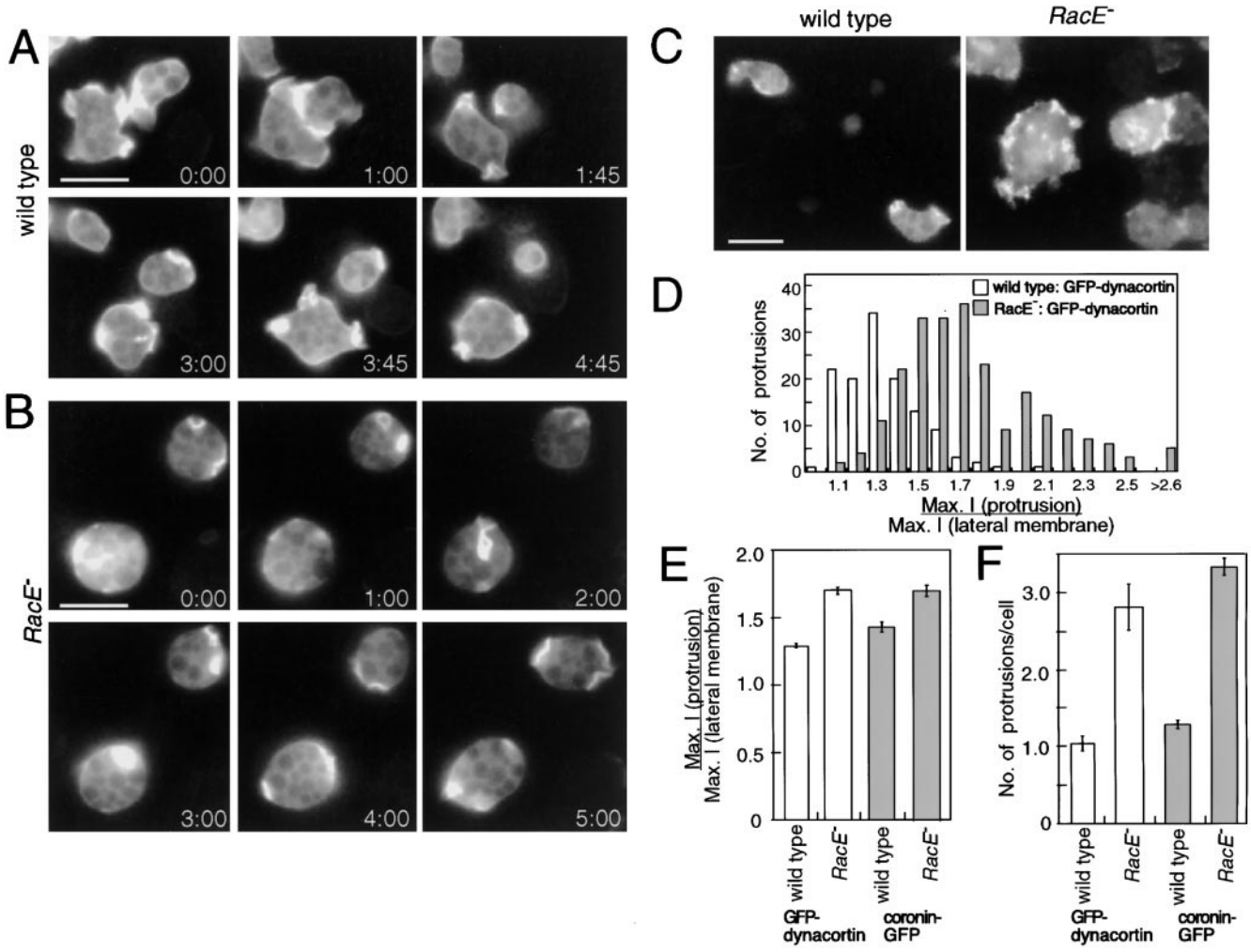

Figure 9. RacE is required for dynacortin and coronin localization. A, GFP-dynacortin localizes to the cell cortex and enriches dynamically in the protrusive domains of the wild-type (parental DH1) cells. B, In the *RacE*$^-$ (24EH6) cell, GFP-dynacortin concentrates in the protrusive domains of the cells. Numbers in A and B are in minutes:seconds. C, Coronin-GFP localizes to the cortex and is enriched in protrusions in wild-type cells. Coronin-GFP is more concentrated in cell surface projections in the *RacE*$^-$ cell line. Bars, 10 μm (applies to all panels in each group). All cells in A–C were imaged alive. D, Determining the ratio of the maximum pixel intensity of the protrusion [Max. I (protrusion)] to the maximum pixel intensity of the lateral membrane [Max. I (lateral membrane)] revealed that GFP-dynacortin is enriched ~28% in the protrusions compared with the lateral membrane in the wild-type cells. In the *RacE*$^-$ cells, GFP-dynacortin is enriched ~70% in the protrusions. By plotting the number of protrusions at each ratio, it is apparent that the populations are distinct distributions. E, The mean ± the SEM are displayed for the cell lines. The differences between each pair of populations are significant (*t* test: $P < 0.0001$). The ratios were determined for cells imaged for a period of time up to 10 min. Therefore, the distributions were determined by making the measurements for a total of protrusions formed over time by m cells. Wild-type:GFP-dynacortin: n = 128, m = 17; *RacE*$^-$:GFP-dynacortin: n = 233, m = 11; wild-type:coronin-GFP: n = 57, m = 13; *RacE*$^-$:coronin-GFP: n = 65, m = 7. F, The *RacE*$^-$ mutant cells also have a greater number of dynacortin- and coronin-rich protrusions on their surfaces compared with the wild-type strain (*t* test: $P < 0.0001$). Number of protrusions was determined by averaging the number of protrusions detected by a single optical view of the cells taken every 30 s for several minutes. This allowed us to accurately count time points in which the cell cortex was quiescent (no apparent protrusion). Therefore, averages were determined from a total of time points taken from m cells. Wild-type: GFP-dynacortin: n = 78, m = 4; *RacE*$^-$:GFP-dynacortin: n = 81, m = 3; wild-type:coronin-GFP: n = 249, m = 13; *RacE*$^-$:coronin-GFP: n = 151, m = 8. Qualitative observations from at least ten of other cells for each genotype were consistent with the quantitative results in D–F.

determined the ratio of the maximal pixel intensity in the protrusion to the maximal pixel intensity of the lateral cortex, using the Metamorph Software Package (see Materials and Methods). GFP-dynacortin and coronin-GFP were significantly depleted from the lateral membranes and concentrated in the protrusions in the *RacE* mutant cells (Fig. 9, D and E). Interestingly, the *RacE* mutant cells also formed more dynacortin and coronin-rich protrusions than the parental wild-type cells (Fig. 9 F). We determined the number of protrusions dynamically, which allowed us to determine the percentage of time spent with a particular number of protrusions. The distribution of percentage of time versus the number of protrusions was monomodal for all genotypes. One interesting observation revealed by examining the data in this manner was that the parental wild-type cells spent ~20–30% of the time with no apparent protrusions, whereas the *RacE* mutant cells were without protrusions only 2–4% of the time.

Discussion

Library Complementation/Multicopy Suppression

With the wealth of molecular tools available for the study of *D. discoideum* (for review see Kay and Williams, 1999), complex genetic interactions between molecules are still difficult to probe. Here, we present the use of cDNA library complementation to isolate a gene mutated in a *D. discoideum* strain and to identify high copy suppressors of the mutant strain. The intrinsic property of any cDNA library to contain partial and full-length clones of a given cDNA actually facilitates the ability to perform gene complementation and suppression and to identify interactions between entire pathways. This has allowed us to identify some novel interactions and to elucidate how apparently distinct molecular pathways interact to promote cytokinesis. In a separate study, we have applied this strategy to the study of how cells transit from vegetative growth to differentiation and have identified several new genes that operate in this transition (Robinson, D.N., G.M. Souza, and J.A. Spudich, unpublished data). Thus, this methodology should prove to be a powerful complement to the repertoire of molecular and biochemical techniques available for *D. discoideum*.

Genetics of Global Cortical Stiffness/Tension and Cell Shape Control

In *D. discoideum*, several genes are required for cytokinesis and to generate cortical stiffness of the cell, which contributes to the basal control of cell shape during interphase and morphogenesis. RacE (Larochelle et al., 1997; Gerald et al., 1998) and coronin (deHostas et al., 1993) are distributed globally around the cell throughout the cell cycle. Loss of either RacE or coronin results in a cytokinesis defect. The *RacE* mutant cells have reduced global cortical tension and cannot undergo cytokinesis when grown in the absence of adhesion (Gerald et al., 1998). The *coronin* mutant cells, in contrast, have defects under adhesive and nonadhesive conditions (deHostas et al., 1991; this paper). Since each of these proteins is distributed globally, it suggests that these proteins function in a global system of cortical tension and cell shape control that is essential for cytokinesis.

Dynacortin might also function in the global system for cell shape and cortical stiffness. During cytokinesis, dynacortin is distributed in the cortex globally and even appears somewhat depleted from the cleavage furrow and midbody. Intriguingly, dynacortin was isolated because a fragment of it encoding the COOH half (residues 173–354) suppressed the loss of cortexillin I. Since full-length dynacortin did not rescue the loss of cortexillin I, the COOH fragment of dynacortin might be antagonizing endogenous dynacortin and this antagonism may compensate for the impaired, spatially restricted cortexillin I pathway. The finding that the COOH 2B19 domain disrupts the formation of the wild-type dynacortin complex is consistent with the notion that it antagonizes the wild-type dynacortin function. Overexpression of the full-length dynacortin gene induces a cytokinesis defect in wild-type cells, *cortI*$^{11\text{-}5.1}$ cells, and *myo II*$^-$ null cells. This suggests that myo II and cortexillin I are not required for this dominant effect.

The *coronin* antisense construct was recovered along with the Δ*Ncortexillin I* (cortI 2A19) construct in the predominant clone of cells from the selection experiment, suggesting that a reduction in the level of coronin offered a selective advantage to the *cortexillin I* mutant cell line. Indeed, the *coronin* antisense construct inhibits expression of the coronin protein. Consistent with this model, overexpression of coronin in the *cortI*$^{11\text{-}5.1}$ mutant cells caused an increase in the number of large, multinucleated cells. However, overexpression of coronin in wild-type cells increased the growth rate of the cells (Table II). Thus, we cannot exclude the possibility that a cytokinesis-impaired strain might be more sensitive to an increase in overall growth rate. The *myo II*$^-$ and *RacE* null cells were not sensitive to overexpression of coronin, arguing against this. However, these mutants are derived from different parental *D. discoideum* strains so one cannot rule out strain differences. An alternate interpretation of this result is that since the *coronin* antisense construct produced a *coronin*$^-$ mutant phenotype, the Δ*Ncortexillin I* construct can rescue a *coronin*$^-$, *cortexillin I*$^-$ double mutant strain's defect for growth in suspension. In either case, this particular genetic interaction experiment is nonintuitive and is an example of one of the surprising results from interaction genetic studies.

Both coronin and dynacortin colocalize in the cortex and are coenriched in protrusive domains. The normal cortical localization of both proteins depends on RacE and in the absence of RacE, they become concentrated in the protrusions. It is probable that these are not the only proteins affected by RacE since other actin-binding proteins, such as myo I (Fukui et al., 1989), α-actinin (Furukawa and Fechheimer, 1994), and cofilin (Aizawa et al., 1997), have a related subcellular distribution. However, they provide useful diagnostic markers, which might shed light on why *RacE* mutants have reduced cortical stiffness. Loss of cortical proteins from the lateral cortex (regions between protrusions) may be expected to cause a reduction in cortical stiffness. Intriguingly, dynacortin and coronin are still recruited into protrusive domains efficiently in the *RacE* mutant cells. Other Rac-family small GTPases likely control some aspects of the protrusive activity. RacF1 becomes

enriched in macropinosomes and phagosomes (Rivero et al., 1999), whereas RacE remains uniformly distributed around the cell cortex (Larochelle et al., 1997). In contrast, overexpression of RacC induces ectopic actin-rich protrusions (Seastone et al., 1998). Since many of the cortical cytoskeletal elements are shared between the lateral membrane and many of the actin-rich protrusive structures, different Rac-family proteins may compete for these cortical elements. Thus, it is possible that in the *RacE* mutants, the remaining Rac small GTPases do not have to compete with RacE so that more dynacortin and coronin are recruited into the cortical protrusions.

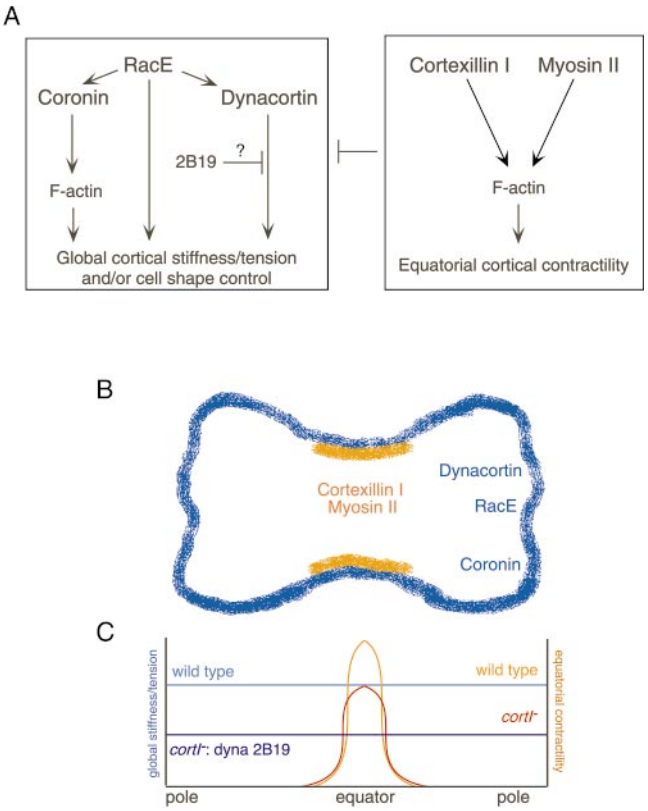

Figure 10. A model of the circuitry of proteins required for cell cleavage. A, A preliminary genetic map for cytokinesis is suggested by multicopy suppression of a cytokinesis-deficient strain of *D. discoideum*. Dynacortin, coronin, and RacE might function in a global pathway for cortical stiffness/tension and cell shape control. Localization of dynacortin and coronin depends on RacE, whereas the localization of dynacortin is independent of coronin. Dynacortin and coronin are drawn on separate branches, although future experiments might uncover a link between them. It is not known how many steps exist between RacE and coronin or dynacortin. Cortexillin I and myo II function in an equatorial pathway to generate spatially restricted contractility. B, A summary of the localization of myo II, cortexillin I, RacE, dynacortin, and coronin during cytokinesis is shown. C, A hypothesis about how the genetic data in this paper might relate to cytokinesis. Cortexillin I and myo II are required at the contractile ring to generate contractility at the furrow. This must overcome a global pathway, breaking the uniformity or symmetry of the cortex for cleavage. Dynacortin may participate in this global pathway that must be overcome by the contractile ring components for cell cleavage. If the equatorial system is impaired (*cortI*$^{-}$), the equatorial contractility is reduced so that it cannot overcome the global system. If the global system is antagonized or lowered (perhaps in *cortI*$^{-}$:dynacortin 2B19), the residual contractile system at the equator may now overcome the global pathway, leading to more efficient cell cleavage.

Global Stiffness/Tension versus Spatial Contractility

Conflicting points of view regarding the mechanism of cytokinesis in the literature include the model of polar relaxation (for example, White and Borisy, 1983) and the model of equatorial stimulation (for review, Rappaport, 1996). In the polar relaxation model, the cell equator maintains a constant cortical tension, whereas the daughter cell pole or body relaxes, allowing the cell to cleave. In the more widely accepted, equatorial stimulation model, the equatorial tension increases through a myo II-dependent mechanism. Both models invoke the formation of a tension differential where the peak resides at the equator or cleavage plane.

One hypothesis indicated by our genetic interaction study suggests a role for the contraction of the equatorial ring to overcome the basal level of global stiffness/tension (Fig. 10). myo II (Moores et al., 1996; Neujahr et al., 1997) and cortexillin I (Weber et al., 1999) are recruited to the contractile ring where they contribute to the contractility of the equator. Both myo II (Pasternak et al., 1989) and the cortexillins (Simson et al., 1998) have been shown to be required for cortical stiffness in interphase cells. During cytokinesis, if the equatorial system is impaired by mutating *cortexillin I*, this can be rescued by fixing the equatorial system by expressing cortexillin I. Alternatively, if dynacortin has a role in global cortical stiffness/tension and cell shape control and is antagonized by dynacortin 2B19 protein, reduction of dynacortin activity may make the global cortex more deformable for the residual equatorial contractile apparatus. While the data presented in this paper do not directly address the mechanical aspects of this hypothesis and certainly other hypotheses can be envisioned, this idea does help to reconcile how a mutant strain defective for contractile ring function can be suppressed by a cortical protein that is enriched in the polar cortex.

We thank Denis Larochelle and Arturo DeLozanne for providing us with the parental and *RacE* mutant cell lines and the RacE cDNA. We thank Eugenio DeHostas for anticoronin antibodies and Jan Faix for the *cortexillin I* deletion strain. We thank members of the Spudich lab for numerous helpful discussions and in particular, Hans Warrick for training in *D. discoideum* techniques.

This work was supported by the National Institutes of Health grant #GM40509 to J.A. Spudich and by a Runyon-Winchell fellowship (#DRG1457) to D.N. Robinson.

Submitted: 7 March 2000
Revised: 20 June 2000
Accepted: 28 June 2000

References

Aizawa, H., Y. Fukui, and I. Yahara. 1997. Live dynamics of *Dictyostelium* cofilin suggests a role in remodeling actin latticework into bundles. *J. Cell Sci.* 110:2333–2344.

Altschul, S.F., T.L. Madden, A.A. Schäffer, J. Zhang, Z. Zhang, W. Miller, and D.J. Lipman. 1997. Gapped BLAST and PSI-BLAST: a new generation of protein database search programs. *Nucleic Acids Res.* 25:3389–3402.

Bezanilla, M., S.L. Forsburg, and T.D. Pollard. 1997. Identification of a second myosin-II in *Schizosaccharomyces pombe*: Myp2p is conditionally required

for cytokinesis. *Mol. Biol. Cell.* 8:2693–2705.
Breckler, J., and B. Burnside. 1994. Myosin I localizes to the midbody region during mammalian cytokinesis. *Cell Motil. Cytoskel.* 29:312–320.
Chang, A.C.M., M.B. Slade, and K.L. Williams. 1990. Identification of the origin of replication of the eukaryote *Dictyostelium discoideum* nuclear plasmid Ddp2. *Plasmid*. 24:208–217.
deHostas, E.L., B. Bradtke, F. Lottspeich, R. Guggenheim, and G. Gerisch. 1991. Coronin, an actin binding protein of *Dictyostelium discoideum* localized to cell surface projections, has sequence similarities to G protein β subunits. *EMBO (Eur. Mol. Biol. Organ.) J.* 10:4097–4104.
deHostas, E.L., C. Rehfueß, B. Bradtke, D.R. Waddell, R. Albrecht, J. Murphy, and G. Gerisch. 1993. *Dictyostelium* mutants lacking the cytoskeletal protein coronin are defective in cytokinesis and cell motility. *J. Cell Biol.* 120:163–173.
DeLozanne, A., and J.A. Spudich. 1987. Disruption of the *Dictyostelium* myosin heavy chain gene by homologous recombination. *Science*. 236:1086–1091.
Devine, J.M., R.A. Firtel, E. Lamar, and W. Rowekamp. 1981. Sequence and expression of the discoidin I gene family in *Dictyostelium discoideum*. *J. Mol. Biol.* 153:273–289.
Faix, J., M. Steinmetz, H. Boves, R.A. Kammerer, F. Lottspeich, U. Mintert, J. Murphy, A. Stock, U. Aebi, and G. Gerisch. 1996. Cortexillins, major determinants of cell shape and size, are actin-bundling proteins with a parallel coiled-coil tail. *Cell.* 86:631–642.
Feinberg, A.P., and B. Vogelstein. 1983. A technique for radiolabeling DNA restriction endonuclease fragments to high specific activity. *Anal. Biochem*. 132:6–13.
Fukui, Y., T.J. Lynch, H. Brzeska, and E.D. Korn. 1989. Myosin I is located at the leading edges of locomoting *Dictyostelium* amoebae. *Nature*. 341:328–331.
Furukawa, R., and M. Fechheimer. 1994. Differential localization of α-actinin and the 30 kD actin-binding protein in the cleavage furrow, phagocytic cup, and contractile vacuole of *Dictyostelium discoideum*. *Cell Motil. Cytoskel.* 29:46–56.
Gerald, N., J. Dai, H.P. Ting-Beall, and A. DeLozanne. 1998. A role for *Dictyostelium* RacE in cortical tension and cleavage furrow progression. *J. Cell Biol.* 141:483–492.
Kay, R.R., and J.G. Williams. 1999. The *Dictyostelium* genome project: an invitation to species hopping. *Trends Genetics*. 15:294–297.
Kitayama, C., A. Sugimoto, and M. Yamamoto. 1997. Type II myosin heavy chain encoded by the *myo2* gene composes the contractile ring during cytokinesis in *Schizosaccharomyces pombe*. *J. Cell Biol.* 137:1309–1319.
Larochelle, D.A., K.K. Vithalani, and A. DeLozanne. 1996. A novel member of the *rho* family of small GTP-binding proteins is specifically required for cytokinesis. *J. Cell Biol.* 133:1321–1329.
Larochelle, D.A., K.K. Vithalani, and A. DeLozanne. 1997. Role of *Dictyostelium* racE in cytokinesis: mutational analysis and localization studies by the use of green fluorescent protein. *Mol. Biol. Cell.* 8:935–944.
Maniak, M., R. Rauchenberger, R. Albrecht, J. Murphy, and G. Gerisch. 1995. Coronin involved in phagocytosis: dynamics of particle-induced relocalization visualized by a green fluorescent protein tag. *Cell.* 83:915–924.
Manstein, D.J., H.-P. Schuster, P. Morandini, and D.M. Hunt. 1995. Cloning vectors for the production of proteins in *Dictyostelium discoideum*. *Gene.* 162:129–134.
McCollum, D., M.K. Balasubramanian, L.E. Pelcher, S.M. Hemmingsen, and K.L. Gould. 1995. *Schizosaccharomyces pombe cdc4*$^{+}$ encodes a novel EF-hand protein essential for cytokinesis. *J. Cell Biol.* 130:651–660.
Moores, S.L., J.H. Sabry, and J.A. Spudich. 1996. Myosin dynamics in live *Dictyostelium* cells. *Proc. Natl. Acad. Sci. USA*. 93:443–446.
Neujahr, R., C. Heizer, R. Albrecht, M. Ecke, J.-M. Schwartz, I. Weber, and G. Gerisch. 1997. Three-dimensional patterns and redistribution of myosin II and actin in mitotic *Dictyostelium* cells. *J. Cell Biol.* 139:1793–1804.
Pasternak, C., J.A. Spudich, and E.L. Elson. 1989. Capping of surface receptors and concomitant cortical tension are generated by conventional myosin. *Nature.* 341:549–551.
Patterson, B., and J.A. Spudich. 1995. A novel positive selection for identifying cold-sensitive myosin II mutants in *Dictyostelium*. *Genetics.* 140:505–515.
Rappaport, R. 1996. Cytokinesis in Animal Cells. Cambridge University Press, Cambridge, UK. 386 pp.
Rivero, F., R. Albrecht, H. Dislich, E. Bracco, L. Graciotti, S. Bozzaro, and A.A. Noegel. 1999. RacF1, a novel member of the Rho protein family in *Dictyostelium discoideum*, associates transiently with cell contact areas, macropinosomes, and phagosomes. *Mol. Biol. Cell.* 10:1205–1219.
Robinson, D.N., and J.A. Spudich. 2000. Towards a molecular understanding of cytokinesis. *Trends Cell Biol.* 10:228–237.
Rogers, S., R. Wells, and M. Rechsteiner. 1986. Amino acid sequences common to rapidly degraded proteins: the PEST hypothesis. *Science*. 234:364–368.
Ruppel, K.M., T.Q.P. Uyeda, and J.A. Spudich. 1994. Role of highly conserved lysine 130 of myosin motor domain. *J. Biol. Chem*. 269:18773–18780.
Ruppert, C., J. Godel, R.T. Müller, R. Kroschewski, J. Reinhard, and M. Bähler. 1995. Localization of the rat myosin I molecules myr 1 and myr 2 and in vivo targeting of their tail domains. *J. Cell Sci.* 108:3775–3786.
Seastone, D.J., E. Lee, J. Bush, D. Knecht, and J. Cardelli. 1998. Overexpression of a novel Rho family GTPase, RacC, induces unusual actin-based structures and positively affects phagocytosis in *Dictyostelium discoideum*. *Mol. Biol. Cell.* 9:2891–2904.
Simson, R., E. Wallraff, J. Faix, J. Niewöhner, G. Gerisch, and E. Sackmann. 1998. Membrane bending modulus and adhesion energy of wild-type and mutant cells of *Dictyostelium* lacking talin or cortexillins. *Biophys. J.* 74:514–522.
Slade, M.B., A.C.M. Chang, and K.L. Williams. 1990. The sequence and organization of Ddp2, a high-copy-number nuclear plasmid of *Dictyostelium discoideum*. *Plasmid*. 24:197–207.
Stock, A., M.O. Steinmetz, P.A. Janmey, U. Aebi, G. Gerisch, R.A. Kammerer, I. Weber, and J. Faix. 1999. Domain analysis of cortexillin I: actin-bundling, PIP_2-binding and the rescue of cytokinesis. *EMBO (Eur. Mol. Biol.) J.* 18: 5274–5284.
Weber, I., G. Gerisch, C. Heizer, J. Murphy, K. Badelt, A. Stock, J.-M. Schwartz, and J. Faix. 1999. Cytokinesis mediated through the recruitment of cortexillins into the cleavage furrow. *EMBO (Eur. Mol. Biol.) J.* 18:586–594.
White, J.G., and G.G. Borisy. 1983. On the mechanisms of cytokinesis in animal cells. *J. Theor. Biol.* 101:289–316.